Ore Geology Reviews 113 (2019) 103112

Contents lists available at ScienceDirect

Ore Geology Reviews

journal homepage: www.elsevier.com/locate/oregeorev

The superlarge Malmyzh porphyry Cu-Au deposit, Sikhote-Alin, eastern Russia: Igneous geochemistry, hydrothermal alteration, mineralization, and fluid inclusion characteristics

Serguei G. Soloviev[a,*], Sergey G. Kryazhev[b], Svetlana S. Dvurechenskaya[b], Vladislav E. Vasyukov[b], Dmitry A. Shumilin[b], Konstantin I. Voskresensky[a]

[a] Institute of Geology of Ore Deposits, Petrography, Mineralogy and Geochemistry (IGEM), Russian Academy of Sciences, 35 Staromonetny Per., Moscow 109017, Russia
[b] Central Research Institute of Geological Prospecting for Base and Precious Metals (TsNIGRI), 1-129 Warshawskoe Chaussee, Moscow 117545, Russia

ARTICLE INFO

Keywords:
Copper
Gold
Porphyry
Fluid inclusions
Sikhote-Alin
Russia

ABSTRACT

The Malmyzh porphyry Cu-Au deposit cluster (> 10 Mt Cu-eq.) is the largest in eastern Russia. It is located in the turbidite terrane and was formed in a transform continental margin setting. The deposit is related to a magnetite-series, dominantly low-K calc-alkaline diorite-tonalite igneous suite, with a higher potassium content in the younger (quartz monzonite to granodiorite) intrusive phases. These metaluminous to peraluminous I-type igneous rocks exhibit slightly elevated Sr/Y and have combined subduction-related to post-subduction geochemical signatures. The magma was emplaced in a series of separated local magmatic "porphyry centres" that vary in petrologic features and relative abundance of different igneous rocks as well as in the dominant development of different hydrothermal alteration and mineralization types. The deposit comprises quartz-K-feldspar ± biotite ± chalcopyrite stockworks in zones of potassic alteration, followed by quartz-magnetite ± chlorite and then by quartz-sulfide-magnetite (with chalcopyrite and bornite) stockworks in zones of propylitic alteration. The latter is partially overprinted by quartz-sericite-chalcopyrite and quartz-sericite-pyrite stockworks formed during phyllic alteration stage. The most productive Cu mineralization is related to a later (quartz-sulfide-magnetite) hydrothermal event during the propylitic alteration stage, and to an early (quartz-sericite-chalcopyrite) event during the phyllic alteration stage. Further development of phyllic alteration caused a dilution of Cu grades. Minor Au, Bi and Te mineralization accompanied Cu mineralization.

Potassic alteration assemblages formed from a homogenous high-salinity (57–78 wt% NaCl and 13–12 wt% KCl), high-temperature (> 525–535 °C), sodic-potassic aqueous-chloride fluid, under a pressure of 500 ± 100 bars. At the propylitic stage, the early quartz-magnetite-chlorite assemblage was formed from a lower temperature (480 ± 5 °C), sodic-dominant aqueous-chloride fluid, under near-critical conditions, and at a similar pressure (~500 bars). This was followed by two episodes of the most intense Cu and Au deposition that occurred under overlapping temperatures (~380 to 250 °C) but from compositionally distinct (sodic-potassic- to sodic-calcic-dominant) boiling to homogenous fluids during the end of the propylitic alteration stage and the beginning of the phyllic alteration stages, respectively. The different cycles of fluid exsolution likely corresponded to degassing of different magmatic intrusions during a multistage magmatic evolution. Corresponding fluid pressure decrease (to ~250 bars and lower) indicates a transition from lithostatic to hydrostatic conditions.

1. Introduction

The Circum-Pacific tectono-magmatic belts possess a great porphyry copper–gold endowment in porphyry systems that have been studied in detail over a large number of deposits, particularly in the southeastern (Andean), northeastern (Cordilleran), and southwestern (Australasian) segments (e.g., Lang et al., 1995; Sillitoe, 1997, 2008, 2010a,b; 2012; Corbett and Leach, 1998; Holliday et al., 2002; Cooke et al., 2005; Garwin et al., 2005; Sillitoe and Perelló, 2005). Compared to these segments, little is still known about porphyry-copper mineralization in the northwestern (Russian) part of the Circum-Pacific. Until most recently, only the world-class Peschanka porphyry Cu-Au-Mo deposit in Chukotka was described in several publications (e.g., Chitalin et al., 2011), and some much smaller porphyry-copper deposits and

* Corresponding author.
E-mail address: serguei07@hotmail.com (S.G. Soloviev).

https://doi.org/10.1016/j.oregeorev.2019.103112
Received 20 May 2019; Received in revised form 30 July 2019; Accepted 2 September 2019
Available online 05 September 2019

occurrences were briefly mentioned in regional reviews (e.g., Nokleberg et al., 1996). However, much greater porphyry Cu-Au to Cu-Au-Mo mineralization was recently discovered in the Northwest Pacific, first, in the large Malmyzh porphyry Cu-Au deposit (e.g., Chitalin et al., 2013). This fueled further interest to porphyry Cu-Au mineralization in the region, with outlining of many other porphyry-copper target areas (e.g., Mihalasky et al., 2015; Petrov et al., 2015; Shashorin et al., 2018; Soloviev et al., 2019).

Gold mineralization in the Malmyzh area has been known since the 1970s (Chernyavsky and Shavkunov, 1976) but for a long time received no attention due to its low metal grades. The porphyry-copper affinity of Malmyzh was proposed in the late 1990 s and confirmed in 2005 by exploration works of Freeport McMoRan/Phelps Dodge Corp. The porphyry-style mineralization was intercept in 2008 by the consortium of Fortress Minerals/IG Copper and Eurasian Minerals Inc. (T. Bowens, M. Canby, A.Volkov, E. Ignatiev, K. Voskresensky, A. Efimov, A. Chitalin and others) (Chitalin et al., 2013; Canby, 2019). Subsequent inferred resource delineation over the four of > 15 mineralized "porphyry centers" known at the deposit yielded 2.54 Gt at average grades of 0.29% Cu and 0.14 g/t Au, or 0.37% Cu-eq., containing 9.29 Mt Cu-eq., or 7.49 Mt Cu and 11.6 Moz Au (0.20% Cu-eq. cut-off; Newall, 2015). Consistently, even by this very partial resource estimate, the deposit corresponds to a "world-class" copper deposit by its tonnage (Singer, 1995) but not the grade (e.g., Cooke et al., 2005). In 2018, the deposit was acquired by the Russian Copper Company. This paper is focused on the deposit genesis based on the new petrologic, mineralogical and fluid inclusion data.

2. Regional tectonic and metallogenic setting

The Malmyzh deposit is situated in the northern part of the Mesozoic Sikhote-Alin orogenic system that extends for over 1500 km along the western Pacific coast and includes a series of terranes accreted to the Asian continental margin during the Paleozoic and Mesozoic (Fig. 1; e.g., Khanchuk et al., 1997, 2016; Nokleberg, 2010; Nokleberg et al., 1996). Following the west-dipping subduction in the Triassic to the Late Jurassic, the accretionary processes occurred during translation along large sinistral strike-slip large fault zones, leading to deposition of turbidite sequences in pull-apart basins during the Late Jurassic to Early Cretaceous. Consistently, from the west to the east, the Jurassic accretionary prism and the Early Cretaceous turbidite terranes are distinguished, the latter reflecting the change from subduction to transform-like translation of the oceanic plate along the continental margin (Fig. 1; Khanchuk et al., 1997).

Khanchuk et al. (2016) distinguished several stages of the tectonic evolution from subduction to transform-like translation. In particular, subduction in the Triassic-Late Jurassic (180–145 Ma) was accompanied by the development of the Jurassic accretionary prism. During the Hauterivian-Aptian (145–125 Ma), the transform plate margin was established, with a strike-slip displacement of the early Paleozoic continental blocks, initiation of turbidite basins, intense deformation of the Jurassic and Early Cretaceous terranes, and development of a slab-window in the subducted slab. The Early Cretaceous turbidite complex is distributed along the boundaries of the Jurassic accretionary prisms, and the corresponding turbidite basins are represented by the Zhuravlevka (in the southern part of the system) and Amur (in the northern part) terranes (Fig. 1). These turbidite basins are composed of Lower Cretaceous (Valanginian to Hauterivian-Aptian) flysh-like sedimentary sequences up to 11 km thick comprising sandstones, siltstones and argillites, with conglomerate, gravelite and mixtite horizons, with minor volcanic rocks (Fig. 1; e.g., Malinovsky, 2011; Malinovsky and Golozubov, 2012).

As noted by Khanchuk et al. (2016), during the late Aptian-early Albian (125–115 Ma), the development of the turbidite basins continued, combined with a *syn*-strike-slip compression caused by a collision with an Early Cretaceous island arc amalgamated to the growing orogenic system from the east. In the late Albian-early Cenomanian (115–95 Ma), further development of the transform margin included the intrusion of calc-alkaline magnesian (S- and I-type) and alkali-calcic ferroan (A-type) granitoids into *syn*-faulting compressional and extensional basins, respectively (Grebennikov et al., 2016). Asthenospheric mantle upwelling through a slab window and subcontinental lithosphere delamination represent the two possible mechanisms to explain the widespread melting of crustal rocks and emplacement of the Early to early Late Cretaceous granitoid suites exhibiting mixed crustal-mantle geochemical signatures (Kruk et al., 2014; Jahn et al., 2015). Khanchuk et al. (2016) emphasized the role of the Central Sikhote-Alin strike-slip fault that caused decompression of the upper mantle along a narrow deep-penetrating zone.

The transform margin tectonic development was accompanied by variable endogenic metallogenic processes that was most intensely expressed in the Central Sikhote-Alin Fault zone. First, this zone is characterized by a broad occurrence of porphyry Cu-Au to Cu-Au-Mo mineralization (e.g., Mihalasky et al., 2015; Soloviev et al., 2019) that is associated with Early-early Late Cretaceous (~100 Ma) porphyry intrusions. The latter vary in composition from shoshonitic (locally with adakitic signature; Sakhno et al., 2011; Soloviev et al., 2019) to tholeiitic, and form discrete clusters, locally in association with coeval volcanic rocks. Second, there are reduced intrusion-related gold (cf. Hart, 2007) and associated W to W-Au deposits in relation to Early-early Late Cretaceous granitoid suites comprising ilmenite-series to transitional ilmenite-magnetite series monzodiorite-granodiorite-granite plutons (Sakhno et al., 2013; Soloviev and Krivoschekov, 2011; Gvozdev et al., 2016; Soloviev et al., 2017a,b; Soloviev and Kryazhev, 2017; Ivin et al., 2017). Slightly younger Late Cretaceous ilmenite-series, granodiorite-granite plutons are accompanied by W-Sn mineralization (e.g., Gonevchuk et al., 2010).

In the Late Cretaceous to Paleogene, subduction resumed in the Eastern Sikhote-Alin orogenic belt, and its subsequent cessation was followed by the development of another system of slab-windows channeling ascent of asthenospheric magma (Khanchuk et al., 1997, 2016). This resulted in the emplacement of younger (72–62 Ma) monzonitic (high-K calc-alkaline to shoshonitic) suites accompanied by Sn-polymetallic deposits resembling the Bolivian tin deposits (Khanchuk et al., 2003; Gonevchuk et al., 2010), and calc-alkaline to monzonitic suites (~65–35 Ma) accompanied by lead–zinc and borosilicate deposits (e.g., Vasilenko, 2004).

3. District geology and mineralization

The Malmyzh mineral district is situated in the Amur terrane, which is underlain by the Lower Cretaceous flysh-like sedimentary sequence subjected to intense deformations, with tight folds and numerous fault zones. These sedimentary rocks were intruded by a number of small stocks of the Early-early Late Cretaceous Lower Amur plutonic suite. According to Vaskin et al. (2009), this suite comprises a variety of magnetite-series plutonic rocks that can be subdivided into several intrusive stages, namely: (1) the early stage comprising intrusive phases of gabbro, monzogabbro, monzonite, diorite, and quartz diorite, (2) the intermediate stage comprising intrusive phases of granodiorite, quartz monzonite, quartz monzodiorite, and granodiorite-porphyry, and (3) the late stage comprising granite-porphyry. The rocks of the early stage dominate and form the majority of the intrusive stocks that outcrop over 2 to 12 km^2, whereas all other rocks occur in much fewer stocks (Vaskin et al., 2009). Vaskin et al. (2009) reported the K-Ar data for the intermediate stage rocks at 100 to 90 Ma. Bukhanova (2018), using the U-Pb method on zircons, dated diorite from the Malmyzh deposit at 128 ± 2 Ma, whereas quartz diorite-porphyry yielded 99.3 ± 1.6 Ma to 96.2 ± 1.9 Ma. In total, these Early-early Late Cretaceous intrusions occur along a hidden northeast-striking structure that merges with the Central Sikhote-Alin Fault further northeast (Figs. 1, 2).

Following the discovery of the Malmyzh deposit, exploration for

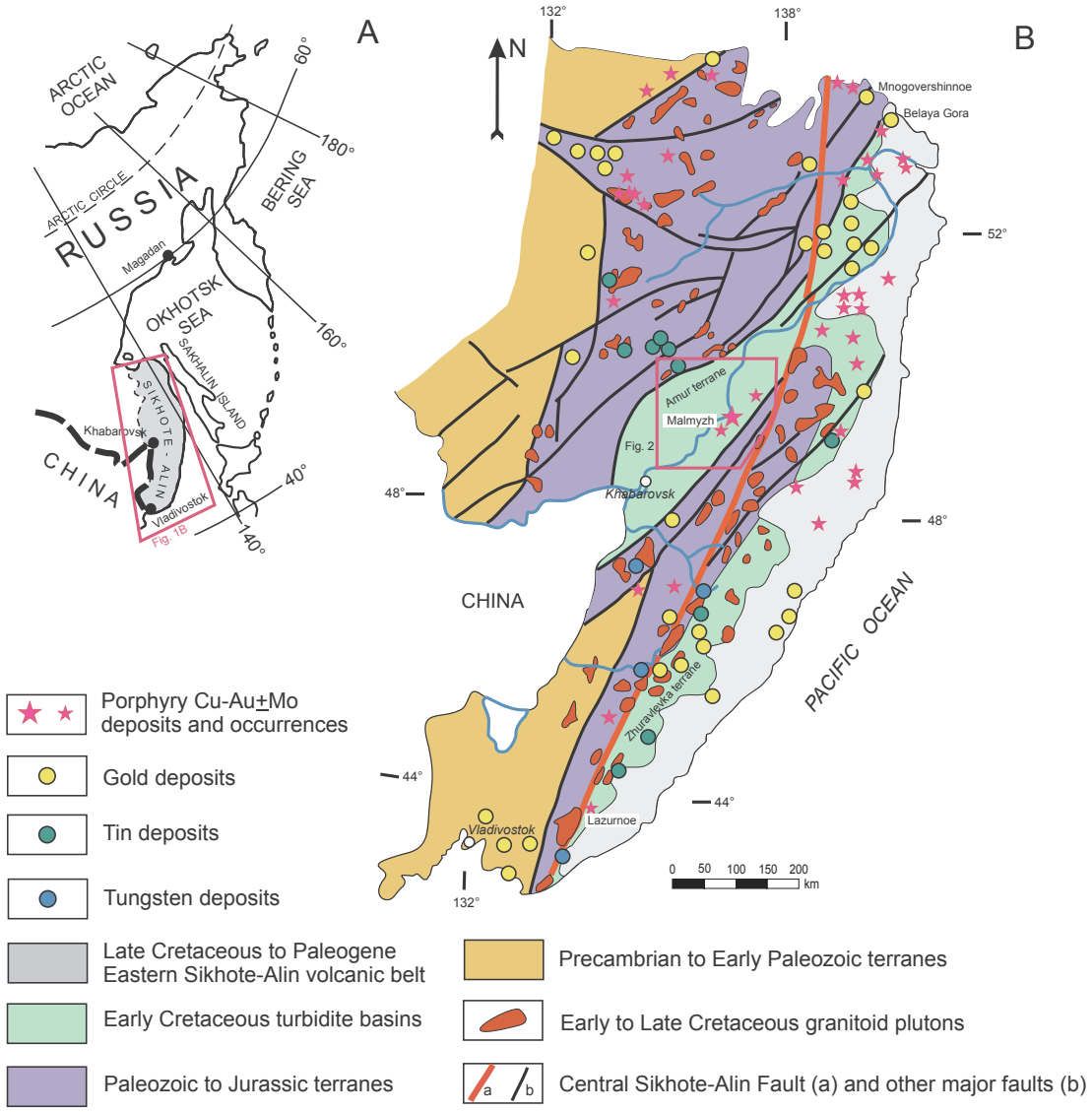

Fig. 1. Regional tectonic setting of the Malmyzh and other porphyry Cu-Au ± Mo deposits, as well as W, Au and Sn deposits, in the Central Sikhote-Alin (geology after Khanchuk et al., 1997, 2016; Vaskin et al., 2009; Belyansky et al., 2011).

porphyry Cu-Au mineralization intensified over the district; this resulted in outlining a number of high-priority targets representing this type of mineralization. In particular, the Poniy cluster of porphyry Cu-Au occurrences and Au veins is situated some 60 km northeast of Malmyzh; its potential resources are currently estimated at > 1 Mt Cu and 160 t Au (Chernyavsky and Sokolov, 2015). The porphyry Cu-Au mineralization is associated with small dioritic stocks, similar to those at Malmyzh. On the other hand, high Bi, As, Sb, W contents in some mineralized zones suggest possible presence of another (reduced intrusion-related gold ?) style of mineralization that contributes to the overall higher (> 2 g/t Au) grades.

Reduced intrusion-related gold mineralization (e.g., Hart, 2007) represents another important style in the district, although so far it includes relatively small (< 10 t Au) occurrences. They comprise quartz-sulfide veins and stockworks in zones of phyllic (quartz-sericite, locally quartz-sericite-tourmaline) to argillic alteration, with dominant arsenopyrite, pyrrhotite, minor pyrite and other sulfides, and variable (low- to high-grade) gold mineralization. These occurrences are associated with small granitoid (typically diorite to quartz diorite) stocks of the Yorokhan and other plutonic suites assigned to Early-early Late Cretaceous and thus being compositionally similar and almost coeval to the intrusions accompanied by porphyry Cu-Au mineralization. Vaskin et al. (2009) reported the 128 Ma K-Ar bulk rock ages, and the U-Pb data on zircons yielded 97.4 ± 6.5 Ma to 101 ± 2 Ma, which is strikingly similar to the data reported by Bukhanova (2018) for some intrusions at Malmyzh. A combination of almost coeval porphyry Cu-Au and reduced intrusion-related Au mineralization styles appears to be typical for other mineral districts in the Central Sikhote-Alin (e.g., Soloviev et al., 2019).

A cluster of large tin-tungsten to tin-polymetallic (Cu, Pb, Zn) deposits is present some 100 km northwest of the Malmyzh deposit area (Figs. 1, 2). These deposits are associated with dominantly Late Cretaceous ilmenite-series, locally high-K monzonitic and granitoid intrusions (Vaskin et al., 2009; Gonevchuk et al., 2010).

4. Deposit geology

The deposit area comprises > 15 separate mineralized zones associated with roughly isometric groups of Early-early Late Cretaceous composite porphyry stocks assigned to the Lower Amur plutonic suite. They intrude Lower Cretaceous siliciclastic, fine-grained, flysh-like package and form small autonomous magmatic centers ("porphyry centers") (Fig. 3). Each "porphyry center" is characterized by small multiphase porphyry stocks, wedged together and rupturing one

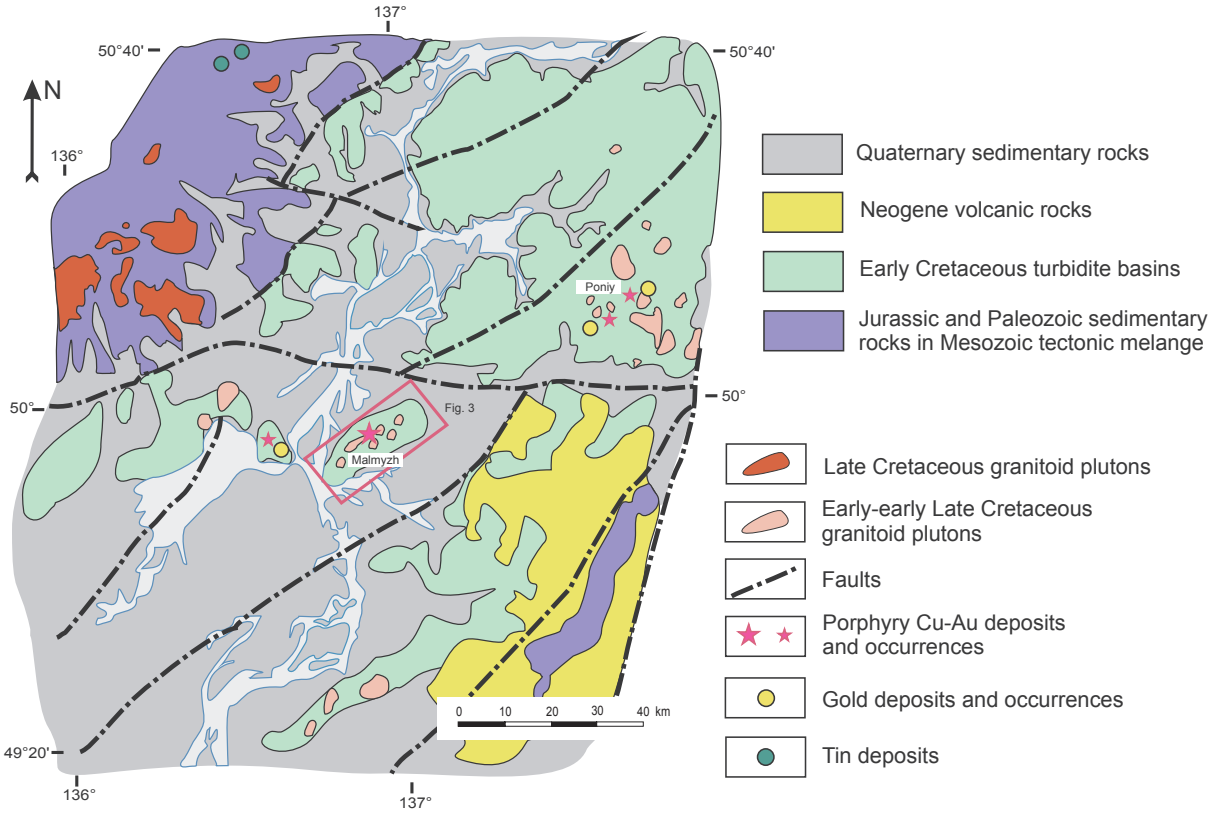

Fig. 2. Geological setting of the Malmyzh deposit area in the Khabarovsk Region (modified after Vaskin et al., 2009).

another, typically with subvertical contacts, locally with dike-like to complex-shaped apophyses. Individual stocks vary in size from 100x100 m to 1 km^2 and more (Chitalin et al., 2013). There are bodies of magmatic (eruptive) breccias in some "porphyry centers" (Fig. 4). The parallel trends of the "porphyry centers" can be traced within a 16x5 km structural "corridor" that extends in the northeastern direction; possible further extensions of this "corridor" are covered by Neogene to Quaternary sediments. These trends, as well as northeast-striking dikes, brecciation zones, and zones of hydrothermal alteration indicate the overall structural control by a wide northeast-striking fault zone, its possible splays and branches, whereas the "porphyry centers" are likely controlled by its intersections with transverse, northwest-striking, hidden linear structures.

The porphyry stocks are accompanied by intense hornfelsing and then by hydrothermal alteration halos, locally with typical "porphyry-style" zonation from the innermost potassic alteration to outer zones of propylitic alteration and overprinting zones of phyllic alteration (e.g., Chitalin et al., 2013). Copper and gold mineralization is roughly coincident with the "inner" propylitic alteration zones overprinting potassic alteration, with copper grades increasing in correlation with a greater chlorite content (Newall, 2015), and additional copper and gold grade increase in local zones of sericite replacement, the latter assigned to the phyllic alteration stage. The "porphyry centers" differ in structural setting of the mineralization; it varies from deep-seated "roots" within the porphyry stocks (Fig. 4A), to that with no distinct "roots" (Fig. 4B), and to occurrence above the "porphyry stocks" in the hosting metasedimentary rocks (Fig. 4C). Some higher-grade Cu-Au intervals appear to be controlled by narrow "pivot" zones of thick quartz-chalcopyrite-magnetite and quartz-pyrite veins (Fig. 4D), and a structural control of higher-grade mineralization by narrower northeast-striking fault zones is locally revealed (Chitalin et al., 2013). Chitalin et al. (2013) reported mineralized intervals varying from 140 m to 474 m in width, with average grades of 0.14 to 0.36% Cu and 0.05 to 0.29 g/t Au. These intervals include narrower zones varying from 18 m to 140 m in width, with average grades of 0.34 to 0.58% Cu and 0.37 to 1.49 g/t Au. Mineralization remains open both in width and to a depth, with many subvertical and angled drill holes varying from > 450 m to > 850 m in length terminated in mineralization. In total, > 0.1% Cu envelope forms oval-shaped to rounded shells, corresponding to the individual "porphyry centers" and varying from ~800 m to > 1600 m along the longer axis and ~200 m to 1000 m across (Newall, 2015). Au/Cu ratio ranges from ~1:4 (Central Zone) to ~3:4 (Freedom Zone) (Canby, 2019).

The mineralization consists of chalcopyrite and minor bornite, with variable but generally minor pyrite, in zones of sulfide dissemination and/or quartz-sulfide to quartz-magnetite-sulfide stockworks. The stockwork density exceeds 30 veinlets per 1 m in the higher-grade (> 0.50% Cu) mineralization and is typically in the range of 10–20 veinlets per 1 m in the ordinary-grade (0.20–0.40% Cu) zones. Quartz-sulfide veinlets are typically 3–10 mm thick; their volume varies from ~ 10 vol% to 30–40 vol%, and sulfide content varies from 0.5 to 1 vol% to 2–3 vol% in zones of ordinary to higher-grade mineralization, respectively. Gold grades are higher in zones with greater pyrite contents. Trace molybdenite occurs occasionally.

Newall (2015) referred to an erosion level of the porphyry system being ~3 km from the paleosurface. This is consistent with a weak development of the late, low-temperature hydrothermal alteration assemblages in the most "porphyry centers" explored to date. This author, however, noted the high-sulfidation minerals (alunite and diaspore) in rocks float in the poorly explored southern part of the deposit area, where the down-faulted uppermost parts of the porphyry-epithermal systems can be located. This provides an opportunity for high-sulfidation epithermal overprint of porphyry mineralization, with corresponding grade increase. This also emphasizes a possible role of post-mineralization tectonism that could have offset and truncated the mineralization.

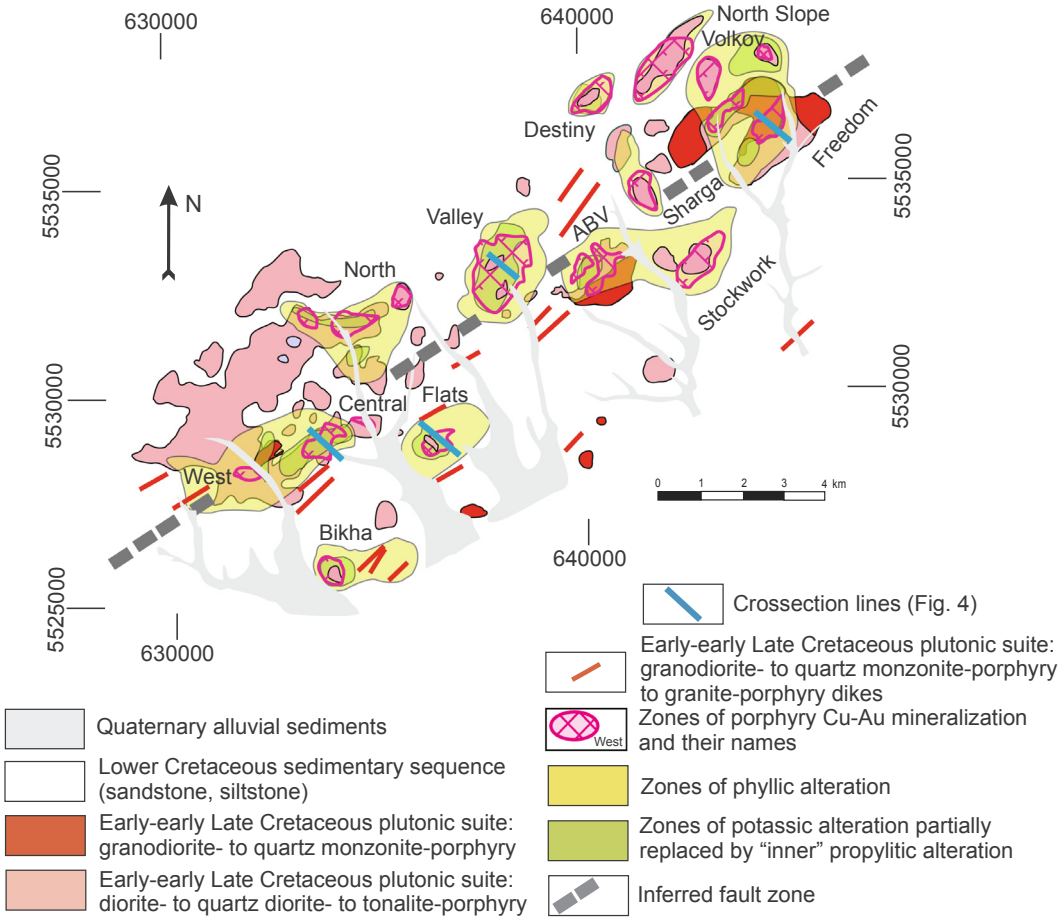

Fig. 3. Geological map of the Malmyzh deposit showing principal mineralized zones (modified after Chitalin et al., 2013; Newall, 2015; Shashorin et al., 2018).

5. Analytical methods

The analyses of igneous rocks were performed in the TsNIGRI Labs, Moscow. SiO_2, TiO_2, Al_2O_3, $Fe_2O_{3\ total}$, MnO, MgO, CaO, K_2O, and P_2O_5, were determined by X-ray fluorescence method. FeO was determined by a wet chemical method (volumetric titration). Powdered samples were analyzed by ICP-MS method for trace elements. Analytical errors are 0.5–5% for major elements and 1–10% for trace elements, depending on the concentrations.

The analyses of minerals were performed using a Cameca SX50 electron probe microanalyser (EPMA) in the GEOKHI Institute of the Russian Academy of Sciences (RAS), Moscow, under operating conditions of 15 kV accelerating voltage, 30nA beam current, with a beam diameter ~3 μm. The accuracy of element measurements was ± 2% rel. for concentrations > 10 wt%, ± 5% rel. for concentrations of 5–10 wt%, ± 10% rel. for concentrations of 1–5 wt%, and ± 15% rel. for concentrations of 0.1–1.0 wt%.

Fluid inclusions were studied in samples from the drill core. Thirty two doubly polished sections (0.3 to 0.5 mm thick) were prepared from 16 individual samples for fluid inclusion petrography and microthermometry. The fluid inclusion study was focused on fluid inclusion assemblages (FIA) of closely associated groups or trails of fluid inclusions with visually similar phase ratios and shapes (Goldstein and Reynolds, 1994). The sequence of entrapment can be inferred from observations of crosscutting trails of FIA along individual fractures or rare primary inclusions distributed randomly within the core of crystals or pseudosecondary trails that are associated with healed microfractures terminated by crystal growth zones (Roedder, 1984). This also enables linking groups of fluid inclusions to various mineralizing stages on the basis of their absence in younger mineral assemblages (Masterman et al., 2005).

Microthermometric analyses were performed using the UMTK-3 freezing-heating stage designed by VIMS Institute and modified by TsNIGRI Institute, to allow low-temperature experiments. Low-temperature measurements were conducted first; cooling was by liquid N_2 flow. The stage employs a chromel–alumel thermocouple and is capable of attaining temperatures ranging from below − 180 to over + 650 °C. The stage was periodically calibrated using the boiling temperature of pure N_2 (−196 °C), triple point for pure CO_2 (−56.6 °C), temperatures of ice melting in standard NaCl solutions (from − 18° to − 1 °C), melting temperatures of $AgNO_3$ (210 °C), K_2CrO_7 (398 °C), and NaI (651 °C). Final ice-melting temperatures were accurate to ± 0.2 °C, eutectic temperatures to ± 1.5 °C, and homogenization temperatures to ± 5 °C. Heating rate (at above 30 °C) was 5 °C/min up to a heating limit at 650 °C.

6. Igneous rocks of the Early-early Late Cretaceous plutonic suite

We observed igneous rocks of at least four to five intrusive phases that appear to represent the 1st and partially 2nd intrusive stages of the Early-early Late Cretaceous Lower Amur plutonic suite. These phases include, from early to late: (1) diorite to quartz diorite-porphyry ("hornblende quartz diorite porphyry" after Newall, 2015) forming larger intrusives, (2) tonalite-porphyry ("quartz-phyric hornblende feldspar porphyry" after Newall, 2015) forming smaller stocks, (3 ?) microtonalite-porphyry ("hornblende feldspar porphyry" after Newall, 2015), which may be in fact a quenched facies of tonalite-porphyry, and (4) granodiorite to quartz monzonite-porphyry, also forming small stocks and dikes. The intrusive sequence is supported by the respective relationships that also indicate the pre- to intermineral intrusions

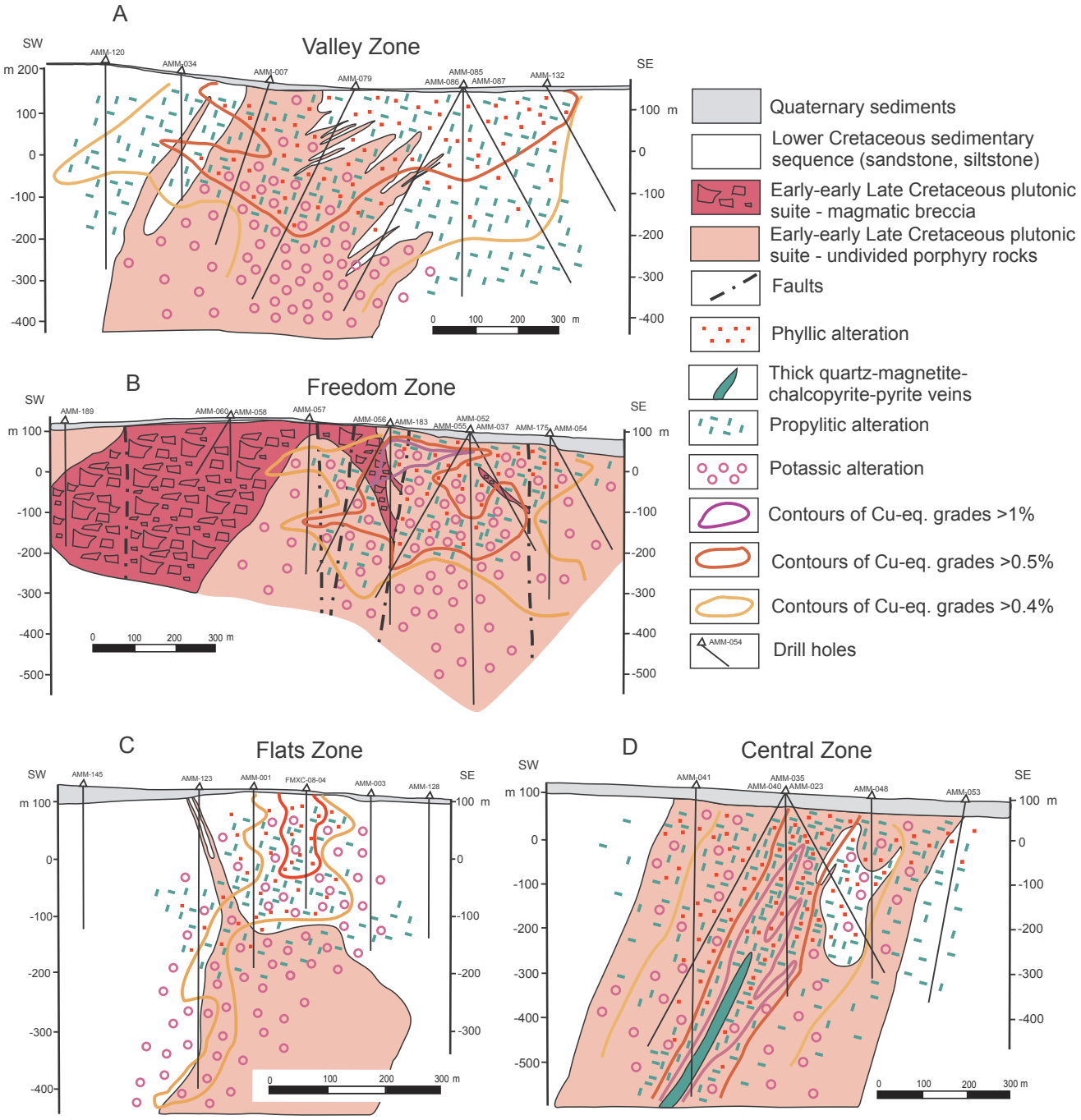

Fig. 4. Cross-sections of some mineralized zones at the Malmyzh deposit (modified after Newall, 2015).

(Fig. 4). Some of the rocks show distinct textural variations suggesting that, in fact, there can be more intrusive phases of similar composition, in the agreement with Newall (2015), who reported at least eight dioritic/tonalitic intrusive phases.

The intrusive rocks are characterized by dominant (55–65 vol%) plagioclase in the groundmass, together with minor fine-grained biotite (5–10 vol% in unaltered varieties) and amphibole (0–15 vol%); K-feldspar in diorite- and tonalite-porphyry is minor (~5 vol%) (Table 1). Plagioclase and/or amphibole are also typical for phenocrysts (Fig. 5A-E), and plagioclase forms phenocrysts even in granodiorite- to quartz monzonite-porphyry, where K-feldspar plays a greater role in the groundmass (20–25 vol%). Quartz is present in tonalite-porphyry, both as phenocrysts (typically rounded to embayed) and in the groundmass (totaling ~ 20 vol%). A lower quartz content (typically ~ 10 vol% or less) occurs in diorite-porphyry. Magnetite is a dominant accessory mineral (2–3 vol% in unaltered varieties); other accessory minerals include apatite, titanite, and zircon. Microtonalite-porphyry forms characteristic microdikes or dikelets ("vein-dikes", after Seedorff et al., 2005) varying from 2 to 3 mm to 10–20 mm in thickness (Fig. 5F-H). Whereas some of the microdikes are intrusions of fluidized magmatic melt, the others appear to be rather due to fracture-controlled, fluid-induced re-crystallization of the host rocks. These microdikes locally contain chalcopyrite in their central (core) zones that can be assigned to magmatic accessory minerals, and form separate small (< 10 m across ?) mineralized stockworks (e.g., Flats Zone). Various clast- to matrix-supported magmatic (phreatic-magmatic, or eruptive) breccias are present, particularly those with microtonalite porphyry to milled clastic-magmatic matrix; in some locations (e.g., Freedom Zone) they

Table 1
Major petrographic features of the Early-early Late Cretaceous igneous rocks (Lower Amur plutonic suite) at the Malmyzh deposit.

Intrusion phases	Rocks	Petrography
1	Diorite-porphyry to quartz diorite-porphyry ("hornblende quartz diorite porphyry")	Medium- to fine-grained mesocratic (grey to greenish-grey) porphyry rock composed of brownish-green amphibole (20–25 vol%), brown biotite (3–5 vol%), plagioclase (60–65 vol %), K-feldspar (~5 vol%), and quartz (5–12 vol%). Phenocrysts are represented by amphibole (15–20 vol%), plagioclase, rarely quartz, and are surrounded by fine- to medium-grained groundmass composed of plagioclase, K-feldspar, quartz, amphibole and biotite. Dominant amphibole phenocrysts are up to 20 mm long and form up to 10 vol%. Tabular plagioclase phenocrysts have a distinct zoning from andesine (45–55 mol.% anorthite in the core) to andesine-oligoclase (rims), and in outer zones contain poikilitic microinclusions of amphibole and biotite. Accessory minerals include magnetite (locally up to 3–5 vol%), titanite, apatite and zircon.
2	Tonalite-porphyry ("quartz-phyric hornblende feldspar porphyry")	Fine-grained mesocratic (grey to greenish-grey) porphyry rock composed of brownish-green amphibole (7–10 vol%), brown biotite (8–10 vol%), plagioclase (60–65 vol%), K-feldspar (~5 vol%), and quartz (10–15 vol%). Phenocrysts form up to 60 vol% of the rock, are represented by plagioclase, rarely amphibole and quartz, and are surrounded by fine-grained groundmass composed of plagioclase, K-feldspar, quartz, amphibole and biotite. Dominant tabular plagioclase phenocrysts are up to 8 mm across and form up to 10 vol%; they have a distinct zoning from andesine (45–50 mol.% anorthite in the core) to andesine-oligoclase (rims). Accessory minerals include magnetite (locally up to 3–5 vol%), titanite, allanite, apatite and zircon.
3 (?)	Microtonalite- porphyry ("hornblende feldspar porphyry")	Fine-grained melanocratic (dark-grey to dark brownish-grey) sharply-porphyry rock composed of brownish-green amphibole (7–12 vol%), biotite (8–10 vol%), plagioclase (55–65 vol%), K-feldspar (~5 vol%), and quartz (10–15 vol%). Phenocrysts are represented by plagioclase and rarely by rounded quartz, and are surrounded by very fine-grained plagioclase-K-feldspar-quartz-biotite-amphibole groundmass. Plagioclase phenocrysts have a distinct zoning from andesine (45–50 mol.% anorthite in the core) to andesine-oligoclase (rims). Accessory minerals include magnetite (locally up to 3–5 vol%), titanite, apatite and zircon.
4 (intramineral mafic dikes)	Monzogabbro-porphyry to quartz monzogabbro porphyry	Fine-grained melanocratic (dark-grey to black) weakly-porphyritic rock composed of biotite (20–25 vol%), plagioclase (50–55 vol%), and quartz (10–15 vol%). Phenocrysts are rare (< 10 vol%), small, and are represented by plagioclase (labradorite), whereas the rock is mostly aphyric and aphanitic. Fine-grained groundmass is composed of plagioclase and quartz, with dark-brown biotite and dense magnetite dissemination. Magnetite and apatite are locally abundant (up to 10 vol% and 2–5 vol%, respectively).
5	Quartz monzonite-porphyry to granodiorite-porphyry	Fine- to medium-grained mesocratic (grey to pinkish-grey to pink) porphyry rock composed of brown biotite (10–15 vol%), plagioclase (40–45 vol%), K-feldspar (15–20 vol%), and quartz (20–25 vol%). Larger phenocrysts are represented mostly by quartz and plagioclase (andesine), smaller phenocrysts – by plagioclase (andesine-oligoclase); they are surrounded by fine- to medium-grained K-feldspar-plagioclase-quartz-biotite groundmass. Plagioclase phenocrysts have a distinct zoning from andesine (in the core) to andesine-oligoclase (rims). Accessory minerals include magnetite (locally up to 3–5 vol%), titanite, rutile, apatite and zircon.

form large (hundreds of meters across; Newall, 2015) bodies (Fig. 4B). An intramineral mafic dike (< 10 cm thick) cutting tonalite porphyry was observed; it can be assigned to lamprophyre (kersantite) or quartz-bearing monzogabbro porphyry (due to plagioclase phenocrysts, although rare). This mafic rock contains abundant apatite (2–5 vol%) and magnetite (~10 vol%), the latter with bornite and chalcopyrite micro-inclusions.

A dataset of the igneous rock analyses was assembled (Table 2); the rock analyses included in the dataset satisfy the criterion on essential immobility of Al and Ti thus supporting the least altered nature of the rocks (Fig. 6A; MacLean and Barrett, 1993), despite of elevated LOI in some analyses. The rocks form a magmatic differentiation trend, ranging from ~ 57 wt% SiO_2 to > 66 wt% SiO_2 (Fig. 6B); subsequent rock phases start with a lower SiO_2 as compared to the most siliceous rocks of previous phases. More differentiated rocks (including granite porphyry; Vaskin et al., 2009) would extend this row toward more siliceous compositions. On the total alkalis vs. SiO_2 diagram (Fig. 6B), the rocks plot mostly in the subalkaline field, whereas quartz monzonite porphyry plot in the midalkaline field, as defined by Middlemost (1997). On the K_2O vs. SiO_2 diagram (Fig. 6C), the rocks plot mostly along the line diving the low-K and medium-K calc-alkaline fields, consistent with their tonalitic compositions, and granodiorite to quartz monzonite porphyry plot in the upper part of the medium-K calc-alkaline field. The rocks are mostly peraluminous and correspond to the peraluminous I-type granites (Fig. 6D; Chappell and White, 1992; Chappell et al., 2012). Consistent with the presence of dominant accessory magnetite, the Fe_2O_3/FeO ratio is > 0.4 in all rock varieties, thus indicating oxidized (magnetite series; Ishihara, 1981) intrusions (Fig. 6E). On the Nb vs. Y diagram (Fig. 6F), less fractionated rocks plot as volcanic arc and syncollisional granite types, whereas more fractionated rocks move toward the post-collisional granite field, thus displaying the pattern, which reflects a fractionation phenomenon (Pearce et al., 1984; Pearce, 1996). Elevated Al_2O_3 (≥ 15 wt%) and Sr (≥ 300 ppm) contents in some rock varieties prompted their examination with respect to the adakitic signatures (Fig. 6G-H; Defant and Drummond, 1990; Martin et al., 2005). As a result, the diorite- and tonalite-porphyry exhibit a weak adakitic affinity due to slightly elevated Sr/Y and low Y values (Fig. 6G). On the other hand, the relatively low Yb_N and La_N/Yb_N values are rather inconsistent with an adakitic signature (Fig. 6H). In primitive mantle-normalized trace element spider diagrams (Fig. 6I), the rocks display strong negative Nb, Ta and Ti anomalies, the latter combined with weak negative Sr and Ba and weak positive Zr and Hf anomalies in the tonalite-porphyry and granodiorite-porphyry. Chondrite-normalized REE diagrams (Fig. 6I) indicate a moderate enrichment in LREE, with a moderately steep overall REE pattern, and no Eu anomalies in the rocks of the early intrusive phases, whereas those of the late phases exhibit a distinct Eu minimum.

7. Hydrothermal assemblages and mineralization

The hydrothermal mineral paragenesis at Malmyzh includes potassic, propylitic, and phyllic alteration assemblages (Fig. 7) occurring

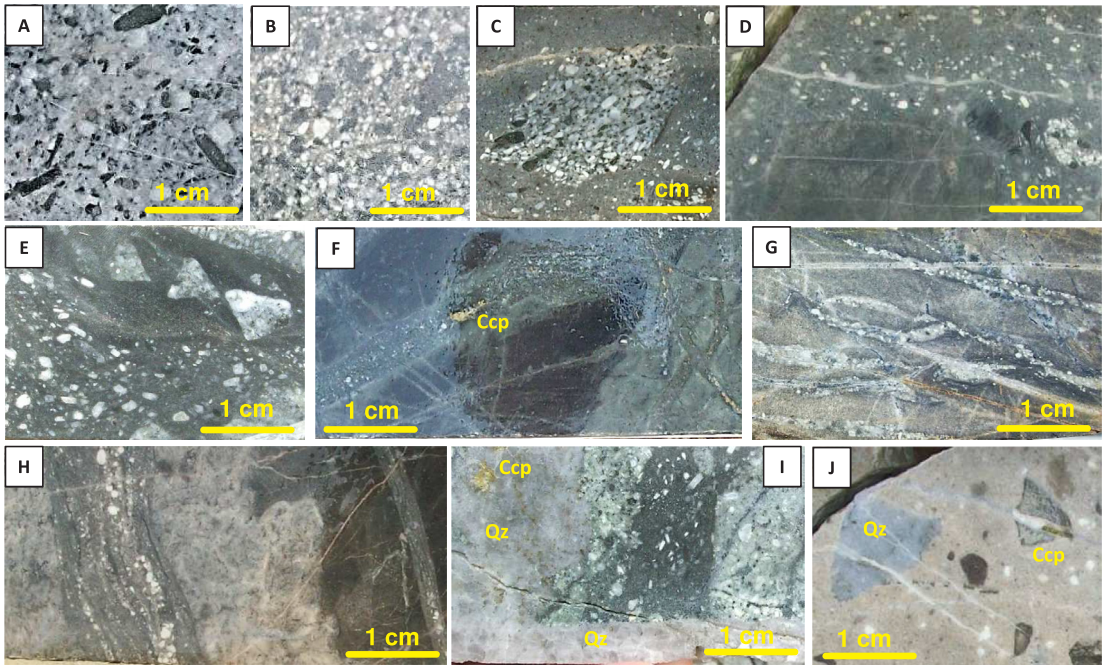

Fig. 5. Photographs showing some typical features of porphyry igneous rocks at the Malmyzh deposit. A. Diorite-porphyry ("amphibole-porphyry") (Central Zone, hole AMM-035). B. Tonalite-porphyry ("plagioclase-porphyry") Central Zone, hole AMM-035). C. Fragment of diorite-porphyry in microtonalite-porphyry (Destiny Zone, hole AMM-69). D. Microtonalite-porphyry contains a large fragment of biotite hornfels (partially overprinted by potassic and propylitic alteration) and a small fragment of diorite-porphyry (Destiny Zone, hole AMM-69). E. Two varieties (phases ?) of microtonalite-porphyry, one with abundant larger plagioclase phenocrysts, another one with small plagioclase phenocrysts, with fragments of diorite-porphyry (Destiny Zone, hole AMM-69). F. Microdikes ("vein-dikes") of microtonalite-porphyry cutting zones of potassic alteration in biotite hornfels and containing central (core) zones of chalcopyrite (Flats Zone, hole AMM-002). G. Microdikes ("vein-dikes") of microtonalite-porphyry cutting zones of potassic alteration in biotite hornfels (Destiny Zone, hole AMM-69). H. Microdikes ("vein-dikes") of microtonalite-porphyry cutting zones of potassic alteration (Valley Zone, hole AMM-114). I. Intrusive breccia with microtonalite-porphyry matrix and diorite-porphyry fragments is cut by quartz to quartz-sericite veinlets with chalcopyrite (Destiny Zone, hole AMM-69). J. Quartz monzonite with plagioclase phenocrysts and fine-grained K-feldspar-dominated groundmass, with angular xenoliths of biotite hornfels and quartz veins with chalcopyrite, is cut by thin quartz-chalcopyrite-carbonate (ankerite) veinlets (Valley Zone, hole AMM-114). Abbreviations: Ccp – chalcopyrite, Qz - quartz.

both as zones of pervasive replacement and systems of quartz-dominant veinlets. Potassic alteration overprints diorite- and tonalite-porphyry, whereas microtonalite-porphyry dikes appear to intersect zones of potassic alteration (Fig. 5F). Granodiorite- to quartz monzonite-porphyry contains fragments of quartz veins likely corresponding to potassic alteration stage but are cut by laminated quartz-magnetite and quartz-ankerite-sulfide veinlets of the propylitic and phyllic alteration stages (Fig. 5J). Narrow intervals of argillic alteration occur locally, in some mineralized zones, and appear to be associated with faults.

7.1. Potassic alteration

This alteration typically occurs in the deeper and central (core) parts of the porphyry-related alteration halos, typically within porphyry stocks, although potassic alteration zones outside these stocks are also present in the host metasedimentary rocks converted to biotite hornfels. The alteration is represented by wide (up to several hundreds of meters across) zones of pervasive replacement, which incorporate stockworks of variously-oriented veinlets and veins and their coalescing selvages. Zones of pervasive replacement are represented by fine-grained patchy to massive fine-grained quartz-biotite and quartz-K-feldspar-biotite aggregate. In the igneous rocks, phenocrysts of mafic minerals are replaced by fine-grained biotite (with minor magnetite and trace chalcopyrite), whereas plagioclase phenocrysts – by K-feldspar. Dark-green amphibole is locally present as well as calcite and plagioclase (oligoclase) indicating sodic-potassic alteration. In the metasedimentary rocks, fine-grained quartz-biotite-K-feldspar ± plagioclase alteration corresponds to biotite hornfels.

Zones of pervasive potassic alteration contain numerous veinlets that have quartz core and dominantly K-feldspar to K-feldspar-biotite selvages, and can be assigned to the A-type (Gustafson and Hunt, 1975; Seedorff et al., 2005; Sillitoe, 2010a) (Fig. 8A-C). These veins vary from barren to those containing minor chalcopyrite, bornite and/or very rare molybdenite; the veinlets with molybdenite appear to be younger than the barren and chalcopyrite-bearing veinlets. Minor magnetite is present in some veinlets and locally contains microinclusions of bornite and chalcopyrite; trace hematite occurs locally (Fig. 9A). Anhydrite is present in quartz-K-feldspar veinlets at deeper levels (Fig. 9A-B). Copper grades in potassic alteration zones unaffected by younger alteration events are < 0.3% Cu (mainly 0.1–0.2% Cu); gold grades are typically < 0.1 g/t Au (occasionally 0.1–0.2 g/t Au).

7.2. Propylitic alteration

Propylitic alteration typically occurs as an outer zone relative to that of potassic alteration. However, marginal and upper parts of potassic alteration zones are clearly overprinted by propylitic alteration, thus revealing that propylitic alteration is a separate hydrothermal stage. Consistently, two different types of propylitic alteration zones are distinguished (cf. Wilson et al., 2003; Corbett, 2017). The "inner" zones are more proximal to porphyry stocks and overprint outer and upper parts of potassic alteration zones. In contrast, the "outer" propylitic alteration zones occur mostly outside porphyry stocks and form an external propylitic alteration halos surrounding potassic alteration zones. Similar to potassic alteration, both pervasive replacement and systems of quartz stockworks are present in the "inner" propylitic alteration zone. Pervasive alteration is expressed in selective replacement of mafic minerals (amphibole and biotite, both primary-magmatic and formed during potassic alteration) by fine-grained chlorite (locally with magnetite and titanite), locally also epidote and newly formed long-

Table 2
Chemical composition of the least altered Early-early Late Cretaceous igneous rocks (Lower Amur plutonic suite) at the Malmyzh deposit (wt.%, ppm).

Rocks	Diorite- to quartz-diorite-porphyry					Tonalite-porphyry			Microtonalite-porphyry		Intramineral mafic dike	Quartz monzonite-porphyry to granodiorite- porphyry			
Sample numbers	80–109	69–394	69–32	65–218	69–264	69–120	69–161.7	69–18	69–326.1	69–17.8	69–120.1	69–169.3	69–145	69–152.8	114–199.3
	1	2	3	4	5	6	7	8	9	10	11	12	13	14	15
wt percent															
SiO_2	58.94	59.09	60.47	61.83	61.83	59.63	61.30	61.55	57.71	62.81	45.80	62.43	64.37	64.53	66.35
TiO_2	0.48	0.44	0.50	0.38	0.38	0.34	0.35	0.41	0.86	0.55	0.84	0.63	0.58	0.50	0.31
Al_2O_3	17.98	18.25	17.98	17.02	16.69	16.94	16.55	16.39	16.43	14.78	15.28	15.24	14.97	14.72	13.90
Fe_2O_3	2.75	2.52	3.62	2.31	3.07	2.38	1.97	3.64	3.05	2.87	13.99	1.72	1.84	1.46	0.84
FeO	3.47	2.82	2.49	2.39	2.76	2.67	2.22	1.93	3.38	1.95	7.85	2.39	2.60	2.52	1.02
MnO	0.08	0.09	0.05	0.09	0.07	0.07	0.06	0.07	0.07	0.05	0.13	0.04	0.05	0.04	0.03
MgO	2.15	2.01	2.22	2.03	1.78	2.15	2.26	2.62	3.13	2.46	2.61	2.48	1.95	2.21	2.35
CaO	6.95	6.56	3.56	6.67	5.13	6.61	5.91	4.49	5.60	4.25	3.60	2.81	3.31	3.56	2.30
Na_2O	3.41	3.73	3.57	3.77	3.64	3.47	3.46	3.69	4.60	4.18	5.50	4.89	5.26	4.52	5.21
K_2O	0.65	0.59	1.09	0.44	0.67	0.85	0.78	1.03	0.54	0.90	0.47	2.54	1.27	0.87	2.82
P_2O_5	0.13	0.14	0.12	0.13	0.12	0.11	0.12	0.13	0.17	0.13	0.15	0.14	0.15	0.11	0.11
LOI	1.80	2.02	3.12	3.07	2.31	4.60	4.59	4.40	3.95	3.66	2.35	3.80	2.33	3.67	3.91
Total	98.79	98.26	98.79	100.13	98.45	99.82	99.57	100.35	99.49	98.59	98.57	99.11	98.68	98.71	99.15
ppm															
Ba	150	156	246	154	126	168	204	306	229	329	381	753	457	353	263
Sr	269	266	343	285	335	271	269	282	282	323	383	405	388	363	227
Co	5.8	8.8	9.9	6.3	8.7	8.4	7.7	8.9	12	9.1	14	8.7	7.3	9.2	7.7
Ni	< 0.5	0.5	3.1	< 0.5	0.6	3.3	1.2	4.8	17.1	11.4	27.8	20.0	16.5	10.6	14.9
V	115	131	162	90	100	138	118	104	148	106	114	101	98	97	68
Cr	3.6	4.7	5.7	4.1	7.9	8.0	24	5.0	57	31	69	43	33	37	32
Li	4.3	6.9	13.3	7.1	8.7	9.0	10.6	10.0	10.6	10.1	17.7	11.9	10.4	10.8	10.3
Rb	7.6	13	31	5.8	11	29	17	26	10.4	23	9.1	46	25	20	24
Be	0.60	0.47	1.1	0.47	0.76	0.76	0.69	0.52	0.72	1.3	1.2	1.5	0.86	1.5	0.94
Zr	69	72	78	92	78	66	63	57	236	178	292	177	164	162	171
Nb	3.4	2.2	3.8	3.1	2.0	3.5	2.6	2.1	6.8	7.3	11	8.1	8.1	8.0	10.8
Y	14	14	20	9.9	14	10.4	14	10.0	18	19	30	24	20	21	21
Sn	< 2.0	< 2.0	< 2.0	< 2.0	< 2.0	< 2.0	< 2.0	< 2.0	< 2.0	< 2.0	< 2.0	< 2.0	< 2.0	< 2.0	< 2.0
Mo	1.1	< 0.1	0.18	0.53	0.25	< 0.1	0.27	0.25	< 0.1	0.27	0.14	0.24	0.31	0.26	0.75
W	0.34	0.19	0.29	0.62	0.19	0.25	0.23	0.15	0.09	0.22	0.28	0.41	0.22	0.58	1.1
Cs	0.18	0.11	1.4	0.20	0.38	1.1	0.70	0.54	0.13	0.41	0.61	1.6	0.53	0.50	0.73
Hf	2.1	2.3	2.3	2.8	2.3	1.9	2.4	1.7	6.7	5.0	8.6	5.2	4.8	4.9	5.4
Ta	0.25	0.07	0.11	0.09	0.16	0.20	0.29	0.16	0.39	0.43	0.93	1.2	1.0	0.90	1.2
Ga	15	15	19	14	16	16	15	15	17	17	20	16	14	15	15
Th	2.8	1.9	2.7	2.1	1.3	2.2	3.3	2.2	12	8.1	21	13	10.3	10.2	12
U	0.70	0.37	0.48	0.59	0.25	0.45	0.88	0.36	1.2	0.85	3.0	2.1	1.1	1.3	1.6
Cu	108	237	2379	23.4	363	582	776	2785	645	2509	1474	1332	2334	859	2465
Zn	42	32	17	37	36	39	35	23	34	4.5	51	1785	17	25	19
Pb	16.6	21.5	16.4	24.9	18.7	8.9	14.5	11.6	19.2	12.9	13.5	8.6	29.5	22.6	27.4
As	< 5.0	< 5.0	< 5.0	< 5.0	< 5.0	< 5.0	8.8	6.0	7.8	< 5.0	< 5.0	6.1	< 5.0	10.3	11.8
Bi	< 5.0	< 5.0	< 5.0	< 5.0	< 5.0	< 5.0	< 5.0	< 5.0	< 5.0	< 5.0	< 5.0	7.5	< 5.0	< 5.0	< 5.0
Sb	< 5.0	< 5.0	< 5.0	< 5.0	< 5.0	< 5.0	< 5.0	< 5.0	6.6	< 5.0	< 5.0	< 5.0	< 5.0	< 5.0	< 5.0
La	10.1	9.4	11	7.9	8.5	7.8	11	8.8	37	26	54	32	26	29	28
Ce	24	23	25	17	20	17	25	20	80	56	118	72	57	65	64
Pr	2.9	2.8	3.4	2.1	2.6	2.1	3.0	2.3	9.2	6.4	13.5	8.2	6.6	7.5	7.3
Nd	12	12	14	8.5	10.8	8.2	12	9.2	34	24	50	30	25	28	27
Sm	2.5	2.4	3.2	1.6	2.3	1.7	2.3	1.7	6.2	4.9	9.1	5.8	4.7	5.2	4.9
Eu	0.77	0.69	0.89	0.54	0.69	0.58	0.64	0.60	1.1	1.1	1.8	1.2	1.0	1.1	0.93
Gd	2.5	2.4	3.3	1.7	2.4	1.6	2.3	1.8	4.9	4.0	7.4	4.8	4.2	4.6	4.3
Tb	0.40	0.41	0.54	0.27	0.38	0.29	0.40	0.28	0.75	0.62	1.1	0.79	0.67	0.69	0.66
Dy	2.6	2.7	3.4	1.7	2.5	1.8	2.5	1.7	4.0	3.8	6.4	4.8	3.8	4.1	3.9

(*continued on next page*)

Table 2 (*continued*)

Rocks	Diorite- to quartz-diorite-porphyry					Tonalite-porphyry			Microtonalite-porphyry		Intramineral mafic dike	Quartz monzonite-porphyry to granodiorite- porphyry			
Sample numbers	80–109	69–394	69–32	65–218	69–264	69–120	69–161.7	69–18	69–326.1	69–17.8	69–120.1	69–169.3	69–145	69–152.8	114–199.3
	1	2	3	4	5	6	7	8	9	10	11	12	13	14	15
wt percent															
Ho	0.57	0.58	0.69	0.40	0.55	0.40	0.56	0.37	0.75	0.77	1.3	1.0	0.78	0.86	0.81
Er	1.7	1.8	2.1	1.2	1.7	1.2	1.7	1.2	2.1	2.1	3.6	3.0	2.2	2.5	2.4
Tm	0.28	0.25	0.34	0.18	0.27	0.21	0.27	0.17	0.32	0.31	0.53	0.42	0.38	0.40	0.32
Yb	1.8	1.8	2.0	1.4	1.9	1.3	1.9	1.2	2.0	2.0	3.4	2.9	2.3	2.6	2.4
Lu	0.29	0.32	0.36	0.24	0.33	0.22	0.30	0.22	0.34	0.30	0.51	0.47	0.39	0.40	0.43

prismatic dark-green amphibole (ferroactinolite to actinolite), whereas feldspars are replaced by fine-grained quartz-magnetite ± albite ± calcite aggregate (Fig. 8D). Magnetite forms fine background dissemination (typically 3–5 vol%, in close association with chlorite and rutile) as well as thin (< 5 mm) and hairline (< 1 mm) veinlets and their stockworks, and generally magnetite content (up to 10 vol%) in zones of propylitic alteration is much greater than that in zones of potassic alteration. Apatite is common in zones of pervasive propylitic alteration; it forms background fine dissemination (~2–3 vol%), particularly in close association with magnetite and fine-grained titanite. Fine-grained, disseminated chalcopyrite and locally minor bornite are present in zones of pervasive propylitic alteration; they appear to occur replacing magnetite (Fig. 9C-F). Fine-grained pyrite is common (~2–3 vol%) and particularly abundant (locally up to 10 vol%) in aggregates with chalcopyrite and magnetite.

Quartz stockworks comprise vein systems of various types. In particular, quartz-chlorite (± epidote, amphibole) veins are common in the "inner" propylitic alteration zones (Fig. 8E-F). Thick (5–20 mm) laminated quartz-magnetite ± chlorite veinlets that can be assigned to the M − type veins (Clark, 1993; Seedorff et al., 2005) (Fig. 8E-I) are also associated with the "inner" pervasive propylitic alteration zones replacing potassic alteration. Minor bornite and chalcopyrite are present in the laminated quartz-magnetite veinlets. A younger vein generation in zones of propylitic alteration is represented by quartz-sulfide-magnetite to quartz-sulfide veins that cut and truncate laminated quartz-magnetite veins (Fig. 8J) and contain less to no magnetite but more sulfides (chalcopyrite or chalcopyrite + bornite, locally also minor pyrite) (Fig. 8K-L). These quartz-sulfide-magnetite veins can also be laminated, are planar to weakly curved, have no clearly expressed selvages or contain thin albite-rich selvages (indicating sodic alteration), and can be classified as transitional AB-type or a variety of the B-type veins. They represent the major host of Cu mineralization at the deposit. Much thicker (20–25 m) quartz-magnetite-chalcopyrite-pyrite vein zones are locally present (e.g., Central Zone; Fig. 4D) and define the most significant enrichment in Cu (> 1%) and Au (> 1 g/t). Intergrowths of sulfide minerals (chalcopyrite, bornite) with chlorite, epidote and/or amphibole (ferroactinolite to actinolite) are common in these veins. Consistently, propylitic alteration appears to be the major mineralizing event that provides the most significant enrichment in Cu particularly in its "inner" zones. Gold mineralization associated with propylitic alteration is represented by very fine-grained native gold-1 (fineness ~ 980‰) found in magnetite. Lower fineness (850 to 760‰) native gold-2 and electrum (fineness 511–616‰) form microinclusions in chalcopyrite (Fig. 9G-K; Table 3) and can be associated with younger mineral assemblages. Zones of propylitic alteration overprinting potassic alteration contain 0.5–1.5% Cu (mainly 0.3–0.7% Cu), whereas gold grades are typically 0.1–0.3 g/t Au (up to 1 g/t Au).

The "outer" propylitic alteration is more distal and occurs outside porphyry stocks thus replacing metasedimentary rocks, and extends locally to > 1 km away from contacts of porphyry stocks (Fig. 3). It is generally a pervasive alteration zone, whereas quartz (quartz-chlorite, etc.) veinlets are rare to absent. This alteration is weaker than that in the inner zone and is characterized by relatively more abundant epidote and albite, in expense of chlorite and amphibole that are dominant in the "inner" zone. Also, plagioclase (albite) is locally abundant in the "outer" zone, whereas magnetite is rather minor.

7.3. Phyllic alteration

Pervasive phyllic alteration overprints earlier alteration types. In zones of potassic alteration, it results in the replacement of K-feldspar and/or biotite by a fine-grained quartz-sericite to quartz-sericite-carbonate aggregate (Fig. 10A). In the zone of "inner" propylitic alteration, phyllic alteration overprint occurs as a replacement of chlorite and/or feldspars by sericite, with the development of the composite chlorite-sericite-quartz aggregate. The latter differs from the "intermediate

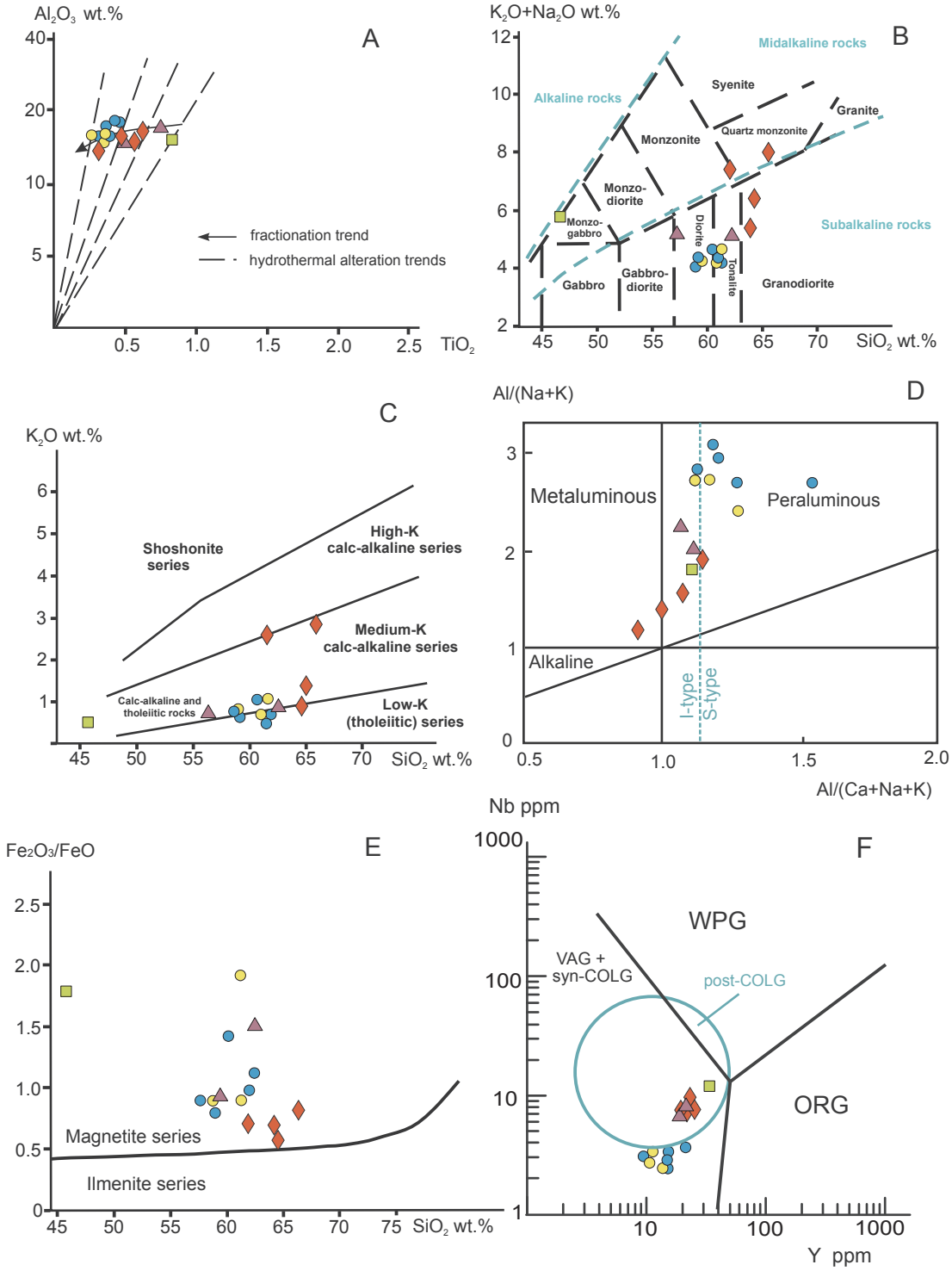

Fig. 6. Plots illustrating the chemistry of igneous rocks at the Malmyzh deposit. (A) Al_2O_3 vs. TiO_2 diagram showing immobility of Al and Ti in the rock samples (MacLean and Barrett, 1993). (B) SiO_2 vs. (K_2O + Na_2O) diagram for chemical compositions of intrusive rocks (after Le Maitre et al., 1989; Middlemost, 1997). (C) SiO_2 vs. K_2O diagram (after Peccerillo and Taylor, 1976; Le Maitre et al., 1989). (D) Al/(Na + K) vs. Al/(Ca + Na + K) diagram defining the alkaline, metaluminous and peraluminous igneous rocks as well as the I- and S-types of granites (after Maniar and Piccoli, 1989; Chappell and White, 1992). (E) Fe_2O_3/FeO vs. SiO_2 diagram defining magnetite- and ilmenite-series rocks (after Ishihara, 1981). (F) Nb vs. Y diagram showing compositional fields of granitic rocks formed in syncollisional (*syn*-COLG), post-collisional (post-COLG), volcanic arc (VAG), within-plate (WPG), and oceanic ridge (ORG) tectonic environments (after Pearce et al., 1984; Pearce, 1996). (G-H) Sr/Y vs. Y and La_N/Yb_N vs. Yb_N diagrams showing compositional fields of adakite and normal calc-alkaline arc rocks (after Defant and Drummond, 1990; Martin et al., 2005; data normalized by REE contents in Cl carbonaceous chondrite after McDonough and Sun, 1995). (I) Primitive mantle-normalized extended trace element spider diagrams (normalization with respect to Sun and McDonough, 1989) and rare earth element chondrite-normalized diagrams (normalization with respect to McDonough and Sun, 1995). The individual rock compositions are from Table 2.

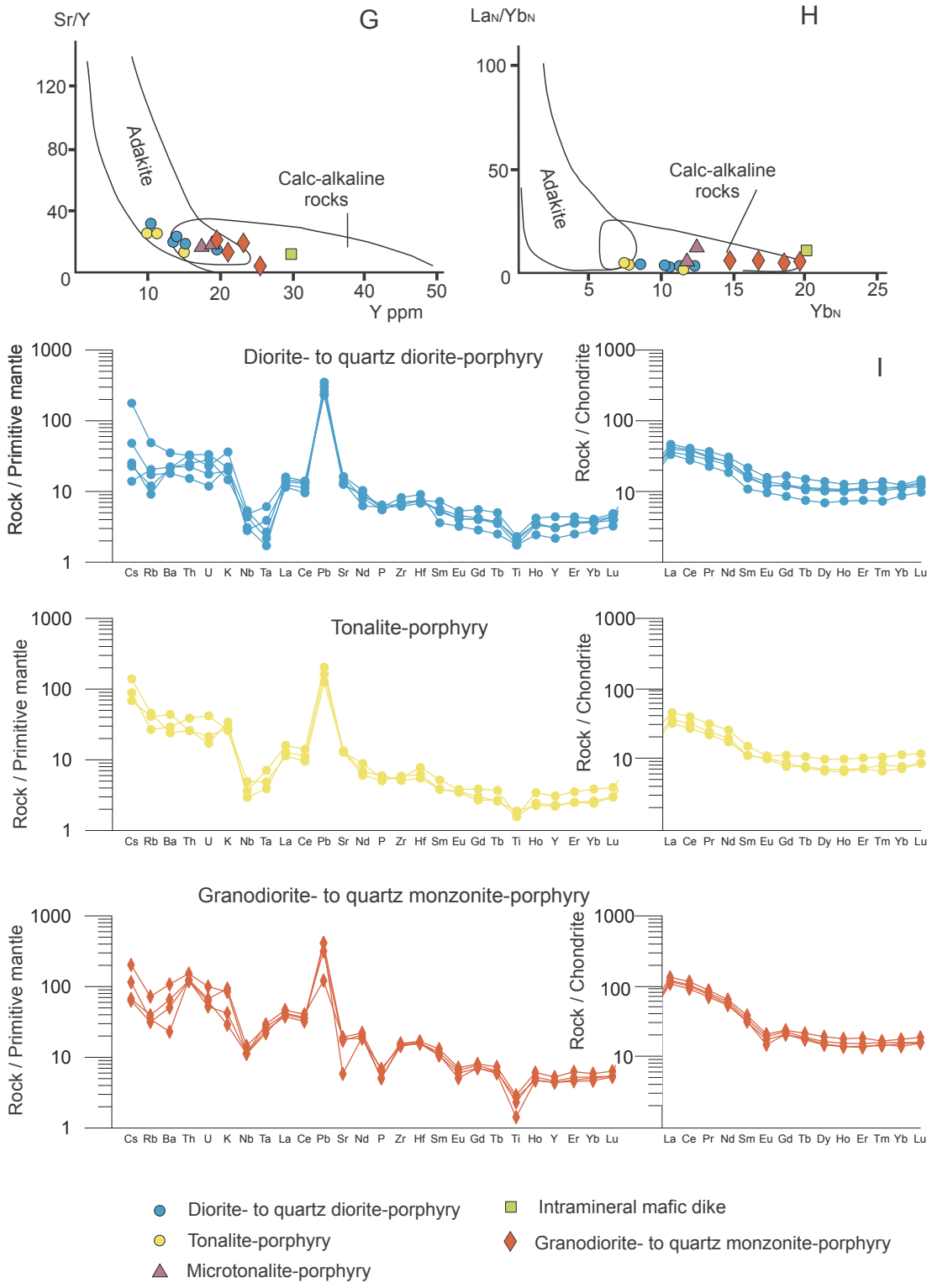

Fig. 6. (*continued*)

argillic alteration" of Sillitoe (2010a) by lack of illite and other clay minerals. Pervasive phyllic alteration of igneous rocks results in the replacement of mafic minerals and feldspars by fine-grained sericite-quartz-carbonate-pyrite aggregate, whereas quartz phenocrysts remain stable. Carbonates include both calcite and Fe-Mg carbonates (siderite, ankerite, dolomite). Fine-disseminated chalcopyrite and pyrite are present in zones of pervasive sericite (quartz-sericite-carbonate) replacement overprinting the "inner" propylitic alteration zones, locally in substantial concentrations (Fig. 10B).

Similar to other alteration assemblages, phyllic alteration zones comprise quartz veins of various types. These include thin variously-oriented quartz ± sericite veinlets reminiscent of the AB- to B-type veins (Fig. 10C-D), thus emphasizing the fact that similar vein types can form across different hydrothermal alteration events (cf. Gregory, 2017; Seedorff et al., 2005). However, K-feldspar and biotite are absent, whereas the presence of sericite ± carbonate in selvages and/or

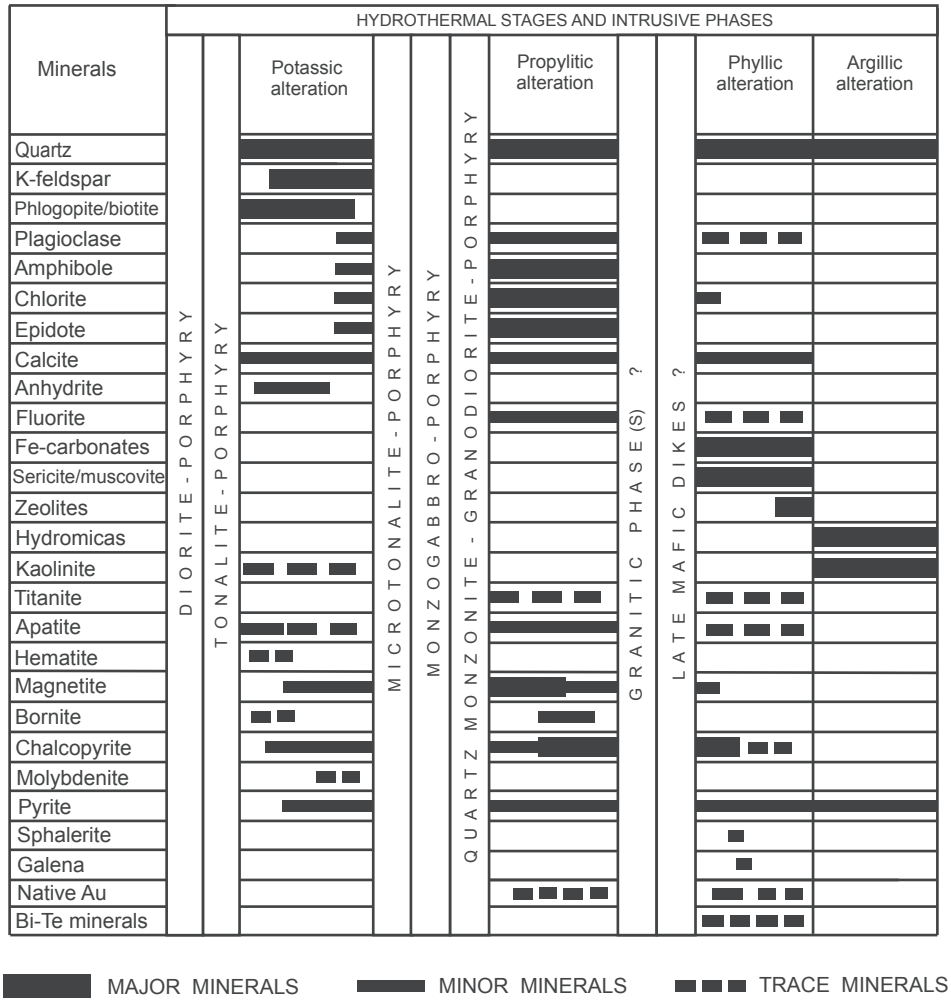

Fig. 7. Sequence of hydrothermal alteration assemblages and intrusive phases at the Malmyzh deposit.

occurrence of these veinlets within zones of pervasive, biotite- and K-feldspar-destructive, quartz-sericite replacement distinguishes them from those assigned to potassic alteration. These veinlets occurring in zones of pervasive quartz-sericite (phyllic) alteration locally contain chalcopyrite (Fig. 10D-E). Quartz-sericite veins cut both quartz-K-feldspar and laminated quartz-magnetite veinlets occurring in the respective alteration zones (Fig. 10F). Trace magnetite is locally present in some quartz-sericite veinlets; however, phyllic alteration is typically magnetite-destructive. Essentially pyritic veinlets are younger (Fig. 10G), and the thicker planar pyrite ± quartz ± sericite veinlets can be classified as the D-type veins (Fig. 10*H*; cf. Gustafson and Hunt, 1975; Seedorff et al., 2005; Sillitoe, 2010a). Zones of massive silicification, typically with ubiquitous pyrite, are also common (Fig. 10I). The latest native gold-3 (fineness ~ 925‰), typically in association with Bi and Te minerals, most distinctly occurs in phyllic alteration zones (Fig. 9L-P; Table 3), whereas part of gold present in the phyllic alteration assemblages is represented by that contained in Au and Au-Ag tellurides.

Phyllic alteration, particularly that expressed in pervasive sericite to quartz-sericite overprint in zones of propylitic alteration, and/or in quartz-sericite veinlets with chalcopyrite, can cause an increase of Cu and Au grades. However, in many other intervals, phyllic alteration, particularly that with high quartz and/or pyrite contents, causes Cu grade dilution. Pyrite forms fine dissemination of irregularly-shaped grains and dominantly cubic crystals in zones of pervasive alteration, with its larger aggregates in zones of silicification and quartz-pyrite veinlets. Minor sphalerite and galena are also common in phyllic alteration assemblages.

8. Fluid inclusion analysis

Fluid inclusions in minerals from the Malmyzh deposit were initially studied by Bukhanova and Plechov (2017), who identified main types of fluid inclusions and defined their P-T-X characteristics. We focused on fluid inclusion assemblages (FIA) assigned to different hydrothermal alteration stages (Table 4), in order to reveal fluid evolution and related processes causing metal deposition.

Porphyry Cu-Au systems typically comprise a central (core) zone of potassic alteration, whereas propylitic alteration comprises “inner” zones that can overprint potassic alteration assemblages (e.g., Corbett, 2017), and “outer” zones that are generally regarded as temporally equivalent to the higher temperature potassic zone (e.g., Wilkinson et al., 2015). Zones of potassic and propylitic alteration are partially overprinted and replaced by phyllic alteration (e.g., Seedorff et al., 2005; Sillitoe, 2010a). Quartz veinlets with different selvages and various magnetite and sulfide content occur in different parts of the porphyry systems and correspond to different hydrothermal alteration stages. Consistently, quartz-K-feldspar ± biotite ± chalcopyrite veinlets are assigned to potassic alteration, whereas quartz-magnetite to quartz-sulfide-magnetite veinlets occurring in propylitic alteration zones - to propylitic alteration assemblage, and quartz-sericite-carbonate to quartz-sericite-chalcopyrite-pyrite veinlets occurring in phyllic alteration zones - to phyllic alteration assemblage (Figs. 8, 10).

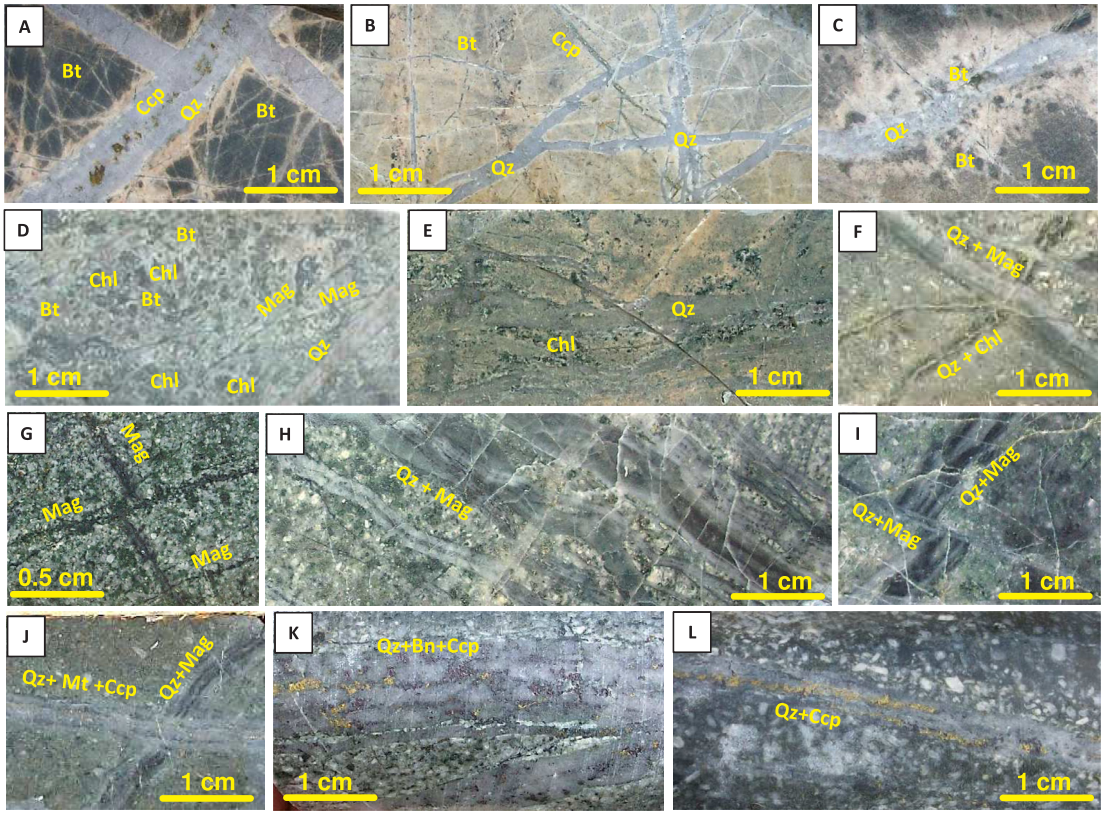

Fig. 8. Photographs showing some typical features of potassic and propylitic alteration assemblages at the Malmyzh deposit. A. Quartz-K-feldspar veinlets with chalcopyrite cutting biotite hornfels (Valley Zone, hole AMM-114). B. Quartz-K-feldspar veinlets in zone of pervasive K-feldspar replacement (after biotite hornfels) (Valley Zone, hole AMM-114). C. Quartz-K-feldspar veinlets with coarse biotite in selvages (Valley Zone, hole AMM-114). D. Pervasive potassic (patchy biotite) replacement, then pervasively replaced by propylitic alteration (chlorite + quartz), with stockwork of thin to hairline magnetite veinlets; everything is cut by thick quartz-chalcopyrite veinlet (Central Zone, hole AMM-035). E. Quartz veinlets with chlorite selvages cut and replace zone of potassic alteration with pink K-feldspar (Flats Zone, hole AMM-002). F. Chlorite veinlet is intersected by laminated quartz-magnetite veinlet (Freedom Zone, hole AMM-037). G. Stockwork of magnetite to magnetite-chlorite veinlets in a zone of pervasive propylitic alteration (North Zone, hole AMM-030). H. Laminated quartz-magnetite veinlets in a zone of pervasive propylitic alteration (Freedom Zone, hole AMM-037). I. Two systems of quartz-magnetite veinlets (thick laminated veinlets are cut by thin veinlets) (Freedom Zone, hole AMM-037). J. Laminated quartz-magnetite veinlet is cut by quartz-magnetite-chalcopyrite veinlets (Freedom Zone, hole AMM-037). K-L. Quartz to quartz-albite-chlorite veinlets with abundant chalcopyrite, bornite and magnetite (Destiny Zone, hole AMM-69). Abbreviations: Ccp – chalcopyrite, Bn – bornite, Mag – magnetite, Mol – molybdenite, Bt – biotite, Chl – chlorite, Qz – quartz. (For interpretation of the references to colour in this figure legend, the reader is referred to the web version of this article.)

8.1. Fluid inclusions in quartz from quartz-K-feldspar ± biotite veinlets (potassic alteration)

Primary and pseudosecondary type 1 fluid inclusions occur in clusters and short trails in quartz from quartz-K-feldspar + biotite veinlets found in zones of potassic alteration (Fig. 11A-D). These inclusions contain a number (5–7) of solid phases including colorless isotropic, typically cubic phases (likely sylvite and halite), hematite (red or orange thin plates), and tabular to prismatic highly to weakly birefringent anisotropic phases, in total occupying 55–75 vol%, and a small- to medium-sized (15–25 vol%) gas bubble (Table 4). The solid phases thought to be halite, sylvite, and hematite, and one more anisotropic phase are systematically present in the fluid inclusions and in relatively constant volume ratios, with constant liquid/vapor/solid ratios and coherent homogenization temperatures, and thus can be considered as daughter minerals (Roedder, 1984). On heating, type 1 inclusions exhibit dissolution of sylvite at 115 ± 5 °C, disappearance of the gas bubble at 480–490 °C, and halite dissolution at 525–535 °C. Hematite and anisotropic phases remain undissolved up to 650 °C (limit of heating). At the temperature of 350–380 °C, hematite shows abrupt darkening and becomes opaque but this effect disappears on subsequent cooling below these temperatures. Due to small amount of liquid, no precise eutectic melting temperature measurement were completed; however, where observed, the eutectic melting temperatures appear to be between −30 and −25 °C. This indicates dominant NaCl and KCl in type 1 inclusions (Crawford, 1981). Using the method of Roedder (1971) for the NaCl-KCl-H_2O system (Fig. 12A), salinity of these inclusions can be defined at 57 to 58 wt% NaCl and 13 to 12 wt% KCl (Roedder, 1971; Sterner et al., 1988; Table 4).

8.2. Fluid inclusions in quartz from quartz-magnetite ± sulfide veinlets in zones of propylitic alteration

Primary and pseudosecondary fluid inclusions occurring in clusters and short trails in quartz from laminated quartz-magnetite to quartz-magnetite-chlorite veinlets found in zones of propylitic alteration are represented by coexisting gaseous-liquid (55–65 vol% gas) type 2A and liquid-gaseous (40–50 vol% gas) type 2B fluid inclusions (Fig. 11E-G). On heating, type 2A inclusions homogenize into gas at 480 ± 5 °C, whereas type 2B inclusions homogenize to liquid at the same temperature. The homogenization occurring by fading meniscus indicates near-critical conditions of the conserved fluid. On warming after freezing, type 2A and 2B inclusions exhibit the eutectic melting temperatures between −25 and −20 °C indicating dominant NaCl and KCl (Crawford, 1981). The final ice melting in type 2A inclusions occurs at −5.8 to −5.1 °C, and in type 2B inclusions - at −8.5 to −7.5 °C. The latter, in the pure NaCl-H_2O system indicates a salinity from 8.0 to 9.0 wt% NaCl-eq. in type 2A inclusions, and a salinity from 11.0 to

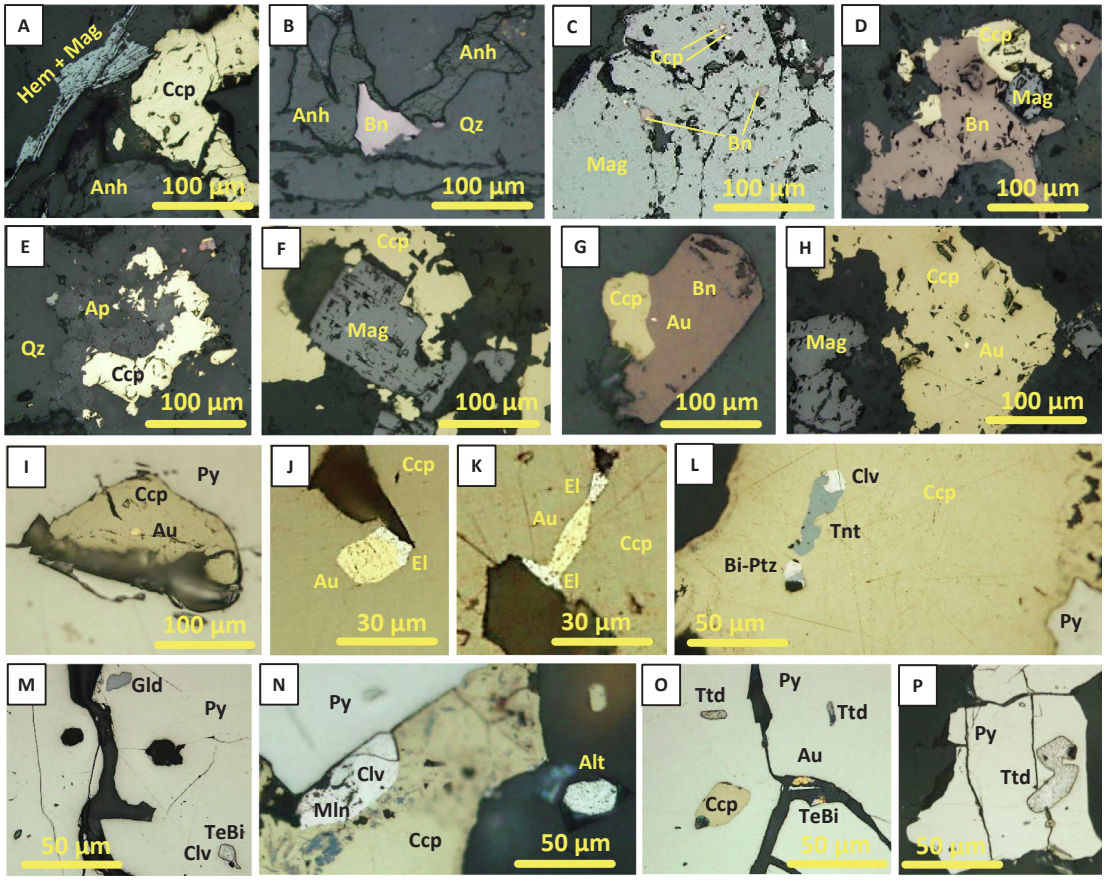

Fig. 9. Photomicrographs of polished sections showing relationships of minerals at the Malmyzh deposit. A. Mushketovite (hematite replaced by magnetite) and chalcopyrite with anhydrite (hole AMM-110). B. Bornite with anhydrite (hole AMM-069). C. Microinclusions of bornite and chalcopyrite in magnetite (hole AMM-069). D. Bornite-chalcopyrite-magnetite intergrowth (hole AMM-69). E. Apatite-chalcopyrite intergrowth (hole AMM-069). F. Magnetite is corroded and replaced by chalcopyrite (hole AMM-075). G. Native gold in bornite partially replaced by chalcopyrite (hole AMM-069). H. Native gold in chalcopyrite associated with magnetite (hole AMM-075). I. Native gold in microinclusion of chalcopyrite in pyrite (hole AMM-114). J-K. Native gold (fineness ~ 830‰) and electrum (fineness ~ 500‰) in chalcopyrite (hole AMM-075). L. Microinclusions of tennantite, Bi-petzite and calaverite in chalcopyrite (hole AMM-114). O. Microinclusions of goldfieldite, calaverite and tellurobismuthite in pyrite (hole AMM-114). N. Calaverite, melonite and altaite in chalcopyrite near euhedral pyrite crystal (hole AMM-114). O. Microinclusions of tetradymite and chalcopyrite in pyrite, and native gold with tellurobismuthite in a microfracture (hole AMM-114). P. Microinclusion of tetradymite in pyrite (hole AMM-114). Abbreviations: Hem – hematite, Mag – magnetite, Py – pyrite, Bn – bornite, Ccp – chalcopyrite, Au – native gold, El – electrum, Clv – calaverite, Alt – altaite, Tnt – tennantite, Gld – goldfieldite, Ttd – tetradymite, TeBi – tellurobismuthite, Bi-Ptz – Bi-petzite, Mln – melonite, Qz – quartz, Anh – anhydrite, Ap - apatite.

12.3 wt% NaCl-eq. in type 2B inclusions (Bodnar and Vityk, 1994; Table 4).

A similar assemblage of primary and pseudosecondary fluid inclusions occurring in clusters and short trails is present in younger quartz-sulfide ± magnetite (with native Au) veinlets in zones of propylitic alteration. This FIA is represented by coexisting gaseous-liquid (60–70 vol% gas) type 3A and liquid-gaseous (30–40 vol% gas) type 3B fluid inclusions (Fig. 11*H*-I). On heating, these inclusions homogenize either to gas (type 3A inclusions) or to liquid (type 3B inclusions) at the temperatures of 410 to 380 °C. On warming after freezing, type 3B inclusions exhibit the eutectic melting temperatures between −26 and −24 °C indicating dominant NaCl and KCl (Crawford, 1981), and the final ice melting at −8.6 to −7.3 °C. The latter, in the pure NaCl-H_2O system, indicates a salinity from 10.9 to 12.4 wt% NaCl-eq. (Bodnar and Vityk, 1994; Table 4). Type 4 liquid-gaseous (10–25 vol% gas) inclusions represent a younger inclusion population (Fig. 11J-M) and are homogenized to liquid at 320–260 °C. The lower-temperature type 4 inclusions occasionally contain an opaque solid phase (Fig. 11M).

8.3. Fluid inclusions in quartz from quartz-sericite veinlets (phyllic alteration)

Primary and pseudosecondary fluid inclusions occurring in clusters and short trails in quartz from quartz-sericite-carbonate-chalcopyrite veinlets are represented by coexisting gaseous (85–95 vol% gas) type 5A and multisolid type 5B fluid inclusions (Fig. 11N-Q). A small opaque (golden-yellow in reflected light) solid phase, with characteristic triangle- to tetrahedron-like appearance, likely chalcopyrite, is present in gaseous type 5A inclusions (Fig. 11N, P). Three solid phases including colorless isotropic, typically cubic phase (halite), prismatic highly to weakly birefringent anisotropic phase, and a small opaque phase (likely chalcopyrite), in total occupying 35–45 vol%, and a medium-sized (20–30 vol%) gas bubble are present in type 5B inclusions. On heating, homogenization (to gas) observed only in several type 5A inclusions due to a small amount of liquid. Overall, type 5A and 5B inclusions homogenize nearly simultaneously over a broad range of temperatures varying from 380 to 250 °C (Table 4). Homogenization in multisolid type 5B inclusions occurs by nearly simultaneous halite and anisotropic phases dissolution and gas bubble disappearance in the most inclusions, or by slightly earlier (for ~ 20 °C) halite dissolution before gas bubble disappearance. Opaque phase remains undissolved up to 650 °C (limit

Table 3
Representative chemical compositions of native gold, and some sulfide, sulfosalt and telluride minerals from the Malmyzh deposit (wt.%).

Minerals	Au	Ag	Cu	S	Se	As	Sb	Co	Ni	Fe	Mo	Re	Total	Empirical formula
Sulfide minerals														
Molybdenite			0.00	42.37	0.02						56.40	0.06	98.85	$Mo_{0.92}S_{2.08}$
Molybdenite			0.00	42.64	0.08						55.45	0.58	98.75	$Mo_{0.91}S_{2.09}$
Molybdenite			0.03	42.10	0.03						55.46	0.86	98.48	$Mo_{0.93}Re_{0.01}S_{2.06}$
Chalcopyrite	0.00	0.00	33.00	35.02	0.02	0.00	0.00	0.04	0.13	30.83			99.04	$Cu_{0.96}(Fe_{1.02}Co_{0.00})_{1.02}S_{2.02}$
Chalcopyrite	0.00	0.01	32.41	35.69	0.04	0.00	0.00	0.31	0.12	31.00			99.58	$Cu_{0.93}(Fe_{1.02}Co_{0.01})_{1.03}S_{2.04}$
Chalcopyrite	0.00	0.05	34.53	35.15	0.02	0.02	0.05	0.23	0.08	28.88			99.00	$Cu_{1.00}(Fe_{0.96}Co_{0.01})_{0.97}S_{2.03}$
Chalcopyrite	0.00	0.08	35.31	35.44	0.00	0.06	0.10	0.10	0.03	28.82			99.94	$Cu_{1.02}(Fe_{0.95}Co_{0.00})_{0.95}S_{2.03}$
Chalcopyrite	0.00	0.07	33.97	35.58	0.01	0.07	0.08	0.21	0.04	29.52			99.54	$Cu_{0.98}(Fe_{0.97}Co_{0.01})_{0.98}S_{2.04}$
Chalcopyrite	0.00	0.12	34.37	35.11	0.03	0.03	0.11	0.21	0.11	29.37			99.47	$Cu_{1.00}(Fe_{0.97}Co_{0.01})_{0.98}S_{2.02}$
Bornite	0.00	0.16	62.15	26.08	0.03	0.00	0.05	0.10	0.01	10.85			99.43	$(Cu_{4.91}Ag_{0.01})_{4.92}(Fe_{0.98}Co_{0.01})_{0.99}S_{4.09}$
Pyrite	0.00	0.00	0.00	52.47	0.09	0.00	0.25	0.31	0.00	44.56			97.68	$Fe_{0.98}Co_{0.01}S_{2.01}$
Pyrite	0.00	0.19	0.15	52.76	0.00	0.00	0.24	0.32	0.15	44.65			98.46	$Fe_{0.98}Co_{0.01}S_{2.01}$
Complex sulfide and telluride minerals														
Minerals	**Zn**	**Ag**	**Cu**	**Hg**	**Te**	**Bi**	**S**	**Se**	**As**	**Sb**	**Ni**	**Fe**	**Total**	Empirical formula
Tennantite	6.56	0.00	41.81	0.30	0.07	0.09	28.13	0.29	18.35	1.89		2.10	93.02	$Cu_{9.84}(Zn_{1.50}Fe_{0.56}Hg_{0.02})_{2.08}(As_{3.66}Sb_{0.23}Bi_{0.01})_{3.91}(S_{13.11}Se_{0.06})_{13.17}$
Goldfieldite	0.00	0.00	45.04	0.19	17.46	1.03	25.26	0.10	3.66	6.44		0.64	99.79	$Cu_{10}(Cu_{1.72}Fe_{0.19}Hg_{0.02})_{1.93}(Te_{2.26}As_{0.81}\ Sb_{0.87}Bi_{0.08})_{4.02}(S_{13.03}Se_{0.02})_{13.05}$
Melonite		0.31	0.47	0.46	78.28	0.30	0.00	0.00			18.84	0.47	99.13	$(Ni_{1.01}Fe_{0.03}Ag_{0.01}Hg_{0.01}Cu_{0.02})_{1.08}Te_{1.92}$
Au-Ag minerals, sulfotelluride and telluride minerals														
Minerals	Au	Ag	Cu	Hg	Te	Bi	S	Se	Pd	Fe	Zn	Pb	Total	Empirical formula
Native Au-1	98.41	0.20	0.14	0.00	0.16	0.00	0.16	0.04	0.22				99.33	
Native Au-2	85.07	10.84	2.85	0.00	0.16	0.17	0.14	0.08	0.16				99.45	
Native Au-2	83.49	14.62	1.20	0.08	0.09	0.08	0.00	0.00	0.16				99.72	
Native Au-2	81.47	15.12	2.71	0.00	0.20	0.00	0.02	0.09	0.08				99.69	
Native Au-2	81.29	15.05	1.36	0.00	0.00	1.37	0.00	0.00	0.00				99.07	
Native Au-2	81.11	14.81	2.64	0.00	0.10	1.28	0.00	0.03	0.00				99.97	
Native Au-2	78.63	18.76	1.38	0.44	0.19	0.00	0.12	0.05	0.00				99.56	
Native Au-2	78.60	17.48	2.73	0.00	0.30	0.21	0.23	0.02	0.16				99.71	
Native Au-2	78.33	19.76	1.52	0.08	0.11	0.00	0.03	0.06	0.00				99.87	
Native Au-2	77.15	16.39	5.37	0.00	0.25	0.00	0.36	0.06	0.28				99.85	
Native Au-2	76.29	21.33	1.39	0.00	0.15	0.00	0.00	0.00	0.07				99.23	
Native Au-2	76.28	21.94	1.25	0.00	0.25	0.00	0.00	0.00	0.09				99.80	
Native Au-2	76.27	21.19	1.51	0.00	0.02	0.00	0.00	0.05	0.06				99.09	
Electrum	61.64	32.58	4.48	0.00	0.48	0.30	0.17	0.12	0.00				99.77	
Electrum	57.89	37.08	3.86	0.00	0.32	0.00	0.18	0.11	0.14				99.58	
Electrum	51.90	44.75	2.29	0.00	0.42	0.09	0.08	0.05	0.00				99.60	
Electrum	51.73	46.25	1.21	0.00	0.18	0.00	0.11	0.11	0.37				99.96	
Electrum	51.24	45.72	1.95	0.00	0.34	0.00	0.08	0.10	0.00				99.43	
Electrum	51.14	45.90	1.67	0.00	0.39	0.00	0.21	0.06	0.08				99.45	
Native Au-3	92.46	6.21	0.27	0.11	0.13	0.00	0.03	0.07	0.22				99.51	
Petzite	24.29	37.05	0.00	0.00	33.77	1.39	0.00	0.08			1.44	1.68	99.70	$Au_{0.96}(Ag_{2.68}Cu_{0.18}Bi_{0.05}Pb_{0.06})_{2.97}\ (Te_{2.06}Se_{0.01})_{2.07}$
Bi-Petzite	20.02	33.68	0.00	0.00	31.98	11.18	0.00	0.14			1.58	0.98	99.56	$Au_{0.81}(Ag_{2.50}Cu_{0.20}Bi_{0.43}Pb_{0.04})_{3.17}\ (Te_{2.01}Se_{0.01})_{2.02}$
Calaverite	41.65	0.03	0.46	0.46	56.24	0.47	0.00	0.00	0.00				99.30	$(Au_{0.96}Ag_{0.00}Bi_{0.01}Hg_{0.01}Cu_{0.03})_{1.01}Te_{1.99}$
Calaverite	40.78	0.25	0.63	0.00	57.06	0.00	0.00	0.00	0.24				98.94	$(Au_{0.93}Ag_{0.01}Cu_{0.04}Pd_{0.01})_{0.99}Te_{2.01}$
Calaverite	39.18	0.42	1.76	0.16	56.98	0.38	0.00	0.00	0.00				98.87	$(Au_{0.88}Ag_{0.02}Bi_{0.01}Hg_{0.00}Cu_{0.12})_{1.03}Te_{1.97}$
Claustalite	0.74	0.30	0.00	0.71	0.10	0.00	3.12	17.80		1.30	0.00	75.50	99.57	$(Pb_{1.01}Au_{0.01}Ag_{0.01}Hg_{0.01}Fe_{0.06})_{1.10}\ (Se_{0.63}S_{0.27})_{0.90}$
Tetradymite	0.08	0.05	0.00	0.44	36.98	56.16	4.64	0.69					99.02	$(Bi_{1.88}Hg_{0.02})_{1.90}Te_{2.03}(S_{1.01}Se_{0.06})_{1.07}$
Tetradymite	0.00	0.38	0.00	0.00	38.00	56.51	4.28	0.54					99.71	$(Bi_{1.90}Ag_{0.02})_{1.92}Te_{2.09}(S_{0.94}Se_{0.05})_{0.99}$
Altaite	0.14	0.24	0.31	0.80	37.67	1.69	0.00	0.00		0.22		57.76	98.83	$(Pb_{0.93}Ag_{0.01}Hg_{0.01}Cu_{0.02}Bi_{0.03}Fe_{0.01})_{1.01}\ Te_{0.99}$
Tellurobismuthite	0.00	0.31	0.00	0.87	47.27	50.59	0.24	0.27	0.00			0.00	99.55	$(Bi_{1.92}Ag_{0.02}Hg_{0.03})_{1.97}\ (Te_{2.94}S_{0.06}Se_{0.03})_{3.03}$
Tellurobismuthite	0.13	0.21	0.00	0.00	46.86	52.26	0.20	0.33	0.00			0.00	99.99	$(Bi_{1.98}Au_{0.01}Ag_{0.02})_{2.01}\ (Te_{2.91}S_{0.05}Se_{0.03})_{2.99}$
Tellurobismuthite	0.00	0.00	0.00	0.00	46.61	52.41	0.27	0.39	0.00			0.00	99.67	$Bi_{1.99}(Te_{2.90}S_{0.07}Se_{0.04})_{3.01}$
Tellurobismuthite	0.00	0.11	0.00	0.34	47.52	50.63	0.29	0.39	0.01			0.51	99.79	$(Bi_{1.91}Ag_{0.01}Pb_{0.02}Hg_{0.01})_{1.95}\ (Te_{2.94}S_{0.07}Se_{0.04})_{3.05}$

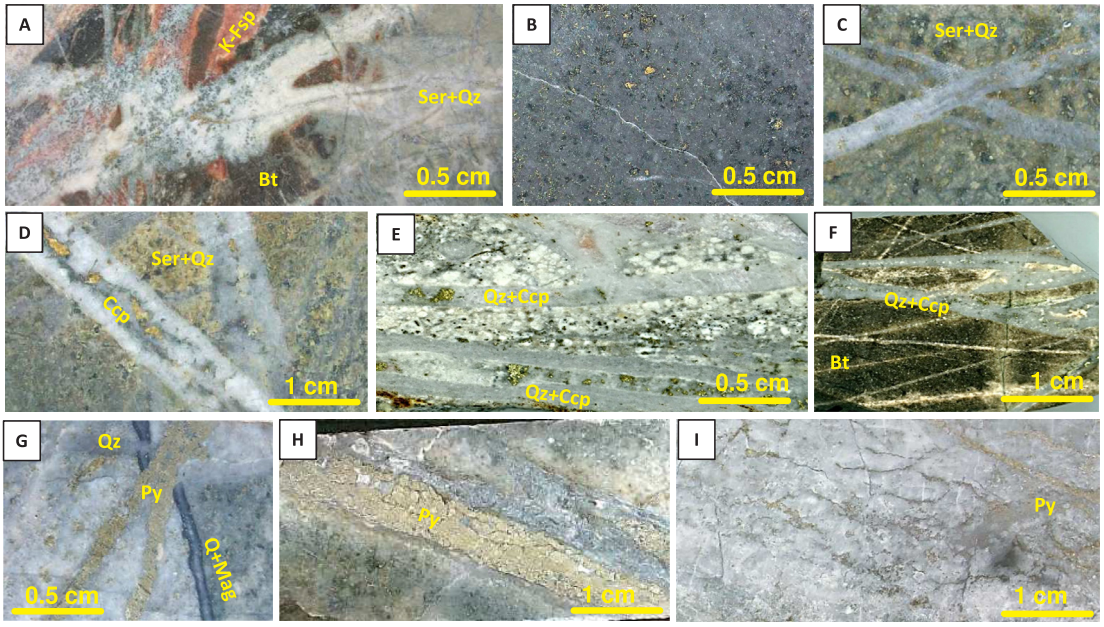

Fig. 10. Photographs showing some typical features of phyllic alteration assemblages at the Malmyzh deposit. A. Potassic alteration zone (K-feldspar and biotite) is cut and partially replaced by quartz-albite-chlorite (propylitic to sodic-propylitic) alteration, which in turn is replaced by a zone of quartz-sericite (phyllic) alteration. (Valley Zone, hole AMM-114). B. Disseminated chalcopyrite in zone of intense propylitic alteration overprinted by phyllic alteration (chlorite-sericite-quartz aggregate) (Freedom Zone, hole AMM-037). C. Quartz veinlets in a zone of pervasive quartz-sericite (phyllic) alteration (Central Zone, hole AMM-035). D. Two generations of quartz-sericite veinlets in a zone of phyllic alteration; the younger veinlet contains chalcopyrite (Central Zone, hole AMM-035). E. Quartz veinlets with chalcopyrite in a zone of phyllic alteration (Valley Zone, hole AMM-130). F. Thin planar quartz veinlets with sericite + carbonate selvages (phyllic alteration) and minor chalcopyrite cut quartz-K-feldspar and K-feldspar veinlets assigned to potassic alteration (Valley Zone, hole AMM-130). G. Quartz-magnetite veinlet (propylitic stage) is cut by quartz veinlet that is cut by pyrite veinlets (Freedom Zone, hole AMM-037). H. Thick quartz-pyrite veinlet in a zone of phyllic alteration (Freedom Zone, hole AMM-037). I. Zone of massive pervasive silicification, with pyrite veinlets and dissemination (Freedom Zone, hole AMM-191). Abbreviations: K-Fsp – K-feldspar, Bt – biotite, Ser – sericite, Mag – magnetite, Qz – quartz, Py – pyrite, Ccp - chalcopyrite.

of heating). The eutectic melting temperatures of around −55 °C measured for type 5B inclusions indicate the presence of $CaCl_2$ (Crawford, 1981). Final ice melting temperatures measured in type 5B inclusions vary from −37 °C to −50 °C. On this basis, salinity estimates in the NaCl-$CaCl_2$-H_2O system (Vanko et al., 1988; Oakes et al., 1990; Fig. 12B) yield a concentration varying from ~ 34 wt% NaCl and 16 wt % $CaCl_2$ to ~ 22 wt% NaCl and 23 wt% $CaCl_2$ (Table 4), indicating a trend of increasing $CaCl_2$ and decreasing NaCl contents toward lower homogenization temperatures (Fig. 12B).

Another FIA of coexisting gaseous (85–90 vol% gas) type 6A and liquid-gaseous type 6B fluid inclusions forms clusters and short trails in quartz from the latest quartz-pyrite ± sericite veins (Fig. 11R). These inclusions homogenize nearly simultaneously either to gas (type 6A inclusions) or to liquid (type 6B inclusions) at the temperatures of 360 to 340 °C (Table 4). On warming after freezing, type 6B inclusions exhibit the eutectic melting temperatures between −27 and –23 °C indicating dominant NaCl and KCl (Crawford, 1981), and the final ice melting at −5.3 to −4.0 °C. The latter, in the pure NaCl-H_2O system, indicates a salinity from 6.5 to 8.3 wt% NaCl-eq. (Bodnar and Vityk, 1994; Table 4).

8.4. Pressure estimate

Minimum pressure can be estimated using homogenization temperatures of multisolid type 1 fluid inclusions that homogenized by halite dissolution. Assuming the slope of the isochores for a 70 wt% NaCl solution is similar to that of the isochores for a 50 wt% NaCl solutions (Atkinson, 2002; Becker et al., 2008), these estimates yield minimum pressures of about 600 bars (Fig. 13; Table 4). Assuming a shallower slope of the isochores for a 70 wt% NaCl solution, these estimates would be lower, approximately at 400 bars, with the overall estimate of 500 ± 100 bars. This pressure corresponds to depths of about 2 km (cf. Fournier, 1999), assuming lithostatic conditions, and it is consistent with the broad development of magmatic crystallization porphyry textures in the igneous plutonic rocks at Malmyzh, together with the lack of coeval (Early-early Late Cretaceous) volcanic rocks in the deposit area. These or similar pressures/depth can be assumed also for the early propylitic alteration assemblages, as fluid boiling near critical conditions, under the temperatures and salinities determined for type 2A and 2B inclusions, corresponds to a pressure of ~ 500 bars (Fig. 14). Lower pressures are envisioned for the late propylitic alteration assemblages, as fluid boiling occurring under the temperatures and salinities determined for type 3A and 3B inclusions corresponds to a pressure of 250 ± 40 bars (Fig. 14), thus indicating a shift toward hydrostatic conditions. The latter pressure appears to be transitional to that during the next, phyllic alteration stage. The respective pressure drop during the propylitic stage and further to the phyllic alteration stage, with the overall trend toward hydrostatic conditions, could be caused by intense faulting and fracturing.

During the phyllic alteration stage, type 5A and 5B fluid inclusion entrapment pressure estimates, considering boiling under NaCl saturation conditions, yield a pressure varying from about 130 bars (fluid inclusions homogenization at 360–380 °C) to ~ 35 bars (fluid inclusion homogenization at 250–270 °C) (Fig. 14). These pressures are significantly lower than those at a depth of 2 km estimated for the propylitic alteration stage. This can reflect a deficiency of these low-pressure estimates, particularly due to the possible presence of minute amounts of CO_2 and other dissolved gases, which would significantly increase a minimum pressure of fluid boiling (Roedder, 1984). For example, in the NaCl-CO_2-H_2O system, under the temperature and salinity conditions determined for type 5 fluid inclusions, the presence of as low as 1 mol.% CO_2, would cause fluid boiling at > 200 bars (Fig. 14). Such a low CO_2 amount cannot be identified by freezing but a presence of CO_2 in the fluid is consistent with the development of

Table 4
Types of fluid inclusions (FI) in minerals from various hydrothermal assemblages of the Malmyzh deposit.

Mineral (number of FI studied)	FI type	FI size, μm	FI content	T_m eu., °C	T_m ice, °C	Homogenization, T_h, °C	Estimated salinity, wt.%	Estimated pressure, bars, and T_h correction, °C
POTASSIC ALTERATION								
Quartz-K-feldspar ± biotite veins								
Quartz (24)	1	< 5–30	15–25 vol% gas, 5–7 solids including sylvite, halite, hematite and anisotropic solids totalling ~ 55–75 vol%	−35 to −25		To liquid: sylvite at 115 ± 5, gas bubble at 480–490, halite at 525–535	NaCl 57-58[a] KCl 13-12[a]	500 ± 100[d] (40–50)
PROPYLITIC ALTERATION								
Laminated quartz-magnetite ± chlorite veins								
Quartz (16)	2A	< 5–20	55–65 vol% gas	−25 to −20	−5.8 to –5.1	To gas at 480 ± 5	NaCl 8.0–9.0[b]	500 ± 10 [e]
Quartz (13)	2B	< 5–20	40–50 vol% gas	−25 to −20	−8.5 to −7.5	To liquid at 480 ± 5	NaCl 11.0–12.3[b]	
Quartz-chalcopyrite-bornite ± magnetite veins								
Quartz (20)	3A	< 5–35	60–70 vol% gas		−0.0 to −0.2	To gas at 380–410	NaCl 0.0–0.4 [b]	250 ± 40[e]
Quartz (20)	3B	< 5–35	30–40 vol% gas	−26 to −24	−8.6 to −7.3	To liquid at 380–410	NaCl 10.9–12.4[b]	
Quartz (25)	4	< 5–30	10–25 vol% gas	−30 to −25	−4.5 to −3.0	To liquid at 260–320	NaCl 5.0–7.2[b]	> 110[f] (< 20)
PHYLLIC ALTERATION								
Quartz + sericite ± chalcopyrite veins								
Quartz (20)	5A	< 5–30	85–95 vol% gas, 0–1 solid (chalcopyrite)			To gas: liquid at 380–250		> 130[f]
Quartz (43)	5B	< 5–35	20–30 vol% gas, 3 solids including halite, chalcopyrite and anisotropic solid totalling ~35–45 vol%	−56 to −54	−50 to −37	To liquid: halite at 355–250, gas at 380–250	NaCl 34, $CaCl_2$ 16[c] to NaCl 22, $CaCl_2$ 23[c]	
Quartz-pyrite + sericite veins								
Quartz (12)	6A	< 5–20	85–90 vol% gas			To gas at 340–360		160 ± 20 [e]
Quartz (8)	6B	< 5–20	30–35 vol% gas	−27 to –23	−5.3 to −4.0	To liquid at 340–360	NaCl 6.5–8.3[b]	

T_m eu. – eutectic temperature (first melting temperature), °C; T_m ice - final ice melting temperature, °C;
[a] Salinity estimated by halite and sylvite dissolution temperatures for the KCl-NaCl-H_2O system (Roedder, 1971; Sterner et al., 1988);
[b] Salinity estimated by final ice melting temperature (Bodnar and Vityk, 1994);
[c] Salinity estimated by halite dissolution temperature and final ice melting temperatures for the NaCl-$CaCl_2$-H_2O system (Vanko et al., 1988; Oakes et al., 1990);
[d] The minimal trapping pressure estimated by using the T_h and halite melting temperature (Atkinson, 2002; Becker et al., 2008);
[e,f] The trapping (e) and minimal (f) pressure estimated by using the salinity and T_h of FI for the NaCl-H_2O system (Atkinson, 2002).

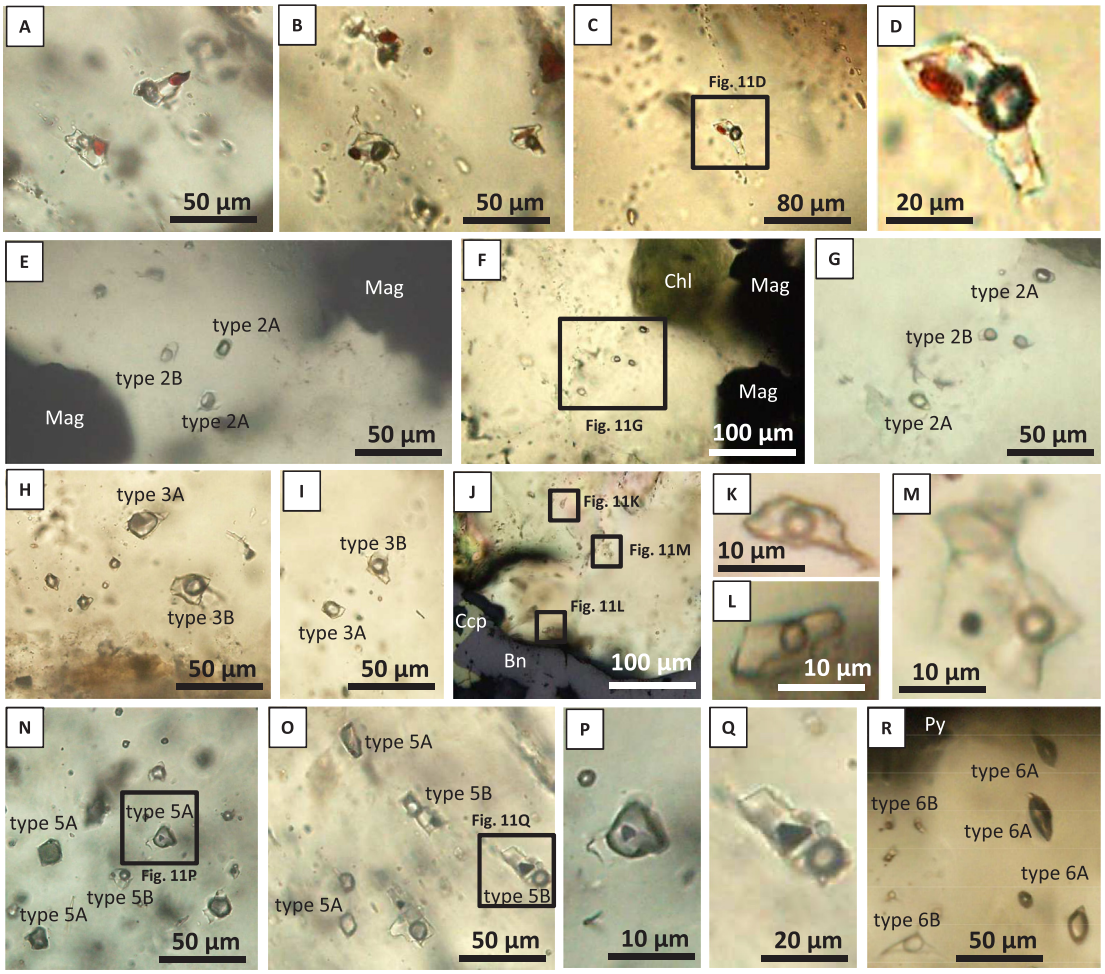

Fig. 11. Types of fluid inclusions in minerals from various hydrothermal alteration assemblages at the Malmyzh deposit. A-D. Multisolid type 1 fluid inclusions containing hematite in quartz from potassic alteration assemblage (D – larger view). E-G. Coexisting gaseous-liquid type 2A and liquid-gaseous type 2B fluid inclusions in quartz from quartz-magnetite-chlorite veinlets (early propylitic alteration assemblage) (G – larger view). H-I. Coexisting gaseous-liquid type 3A and liquid-gaseous type 3B fluid inclusions in quartz from quartz-sulfide ± magnetite veinlets (late propylitic alteration assemblage). J-M. Liquid-gaseous type 4 fluid inclusions in quartz from quartz-sulfide ± magnetite veinlets (late propylitic alteration assemblage) (K-M – larger views). N-Q. Coexisting gaseous type 5A and multisolid type 5B fluid inclusions in quartz from quartz-sericite-chalcopyrite veinlets (phyllic alteration assemblage) (P-Q – larger views showing chalcopyrite crystals both in gaseous (type 5A) and in multisolid (type 5B) inclusions). R. Coexisting type 6A gaseous and type 6B liquid-gaseous fluid inclusion in quartz from quartz-pyrite-sericite veinlet (phyllic alteration assemblage). Abbreviations: Chl – chlorite, Mag – magnetite, Ccp – chalcopyrite, Bn – bornite, Py - pyrite.

carbonate minerals in phyllic alteration assemblages. As a result, the pressure of 130 bar is considered as a minimum pressure that is further consistent with the lack of the Early-early Late Cretaceous volcanic rocks in the deposit area.

9. Discussion

The Malmyzh deposit attracts significant interest because it is a very large porphyry Cu-Au deposit. A discovery of such magnitude highlights the porphyry-copper potential of the large region of eastern Russia and, in a broader sense, the Northwest Pacific. Consistently, revealing features of its location and genesis is important for establishing the geological and genetic model for: (1) improved understanding of similar deposits worldwide and (2) guiding further exploration in the region.

9.1. Tectonic setting and magmatic sources

The transform margin regime commenced in the Central Sikhote-Alin after cessation of active subduction in the Late Jurassic at ~145 Ma, continued during the Hauterivian to Aptian (145–125 Ma), was interrupted by a continent-arc collision in the late Aptian-early Albian (125–115 Ma), and resumed in the late Albian-early Cenomanian (115–95 Ma) (Khanchuk et al., 2016; Grebennikov et al., 2016). The late Albian-early Cenomanian was also the period of the most intense magmatism, with the intrusion of granitoids with mixed crustal-mantle geochemical signatures and locally - intrusions of a shoshonitic magma (Kruk et al., 2014; Jahn et al., 2015). Intense magmatic activity likely corresponded to the development of a slab-window and the respective asthenospheric mantle upwelling and injection (Khanchuk et al., 2016; Grebennikov et al., 2016).

The Malmyzh deposit is associated with the Early-early Late Cretaceous igneous suite (~128 Ma to 99–96 Ma to ~90 Ma; Bukhanova, 2018; Vaskin et al., 2009). Consistently, if the age of ~128 Ma is confirmed, the magmatic emplacement at Malmyzh was likely initiated during the early transform margin stage, was possibly stagnant or interrupted during the continent-arc collision, and resumed and culminated during the further development of the transform margin in the late Albian to early Cenomanian. The long-lasting magmatic evolution and emplacement may explain some subduction-related signatures of the older igneous rocks at Malmyzh, particularly the negative Nb, Ta and Ti as well as Sr and Ba anomalies (Fig. 6I; cf. Pearce et al., 1984). However, elevated Zr and Hf and increasing K contents suggest a more subduction-modified lithospheric mantle source of the

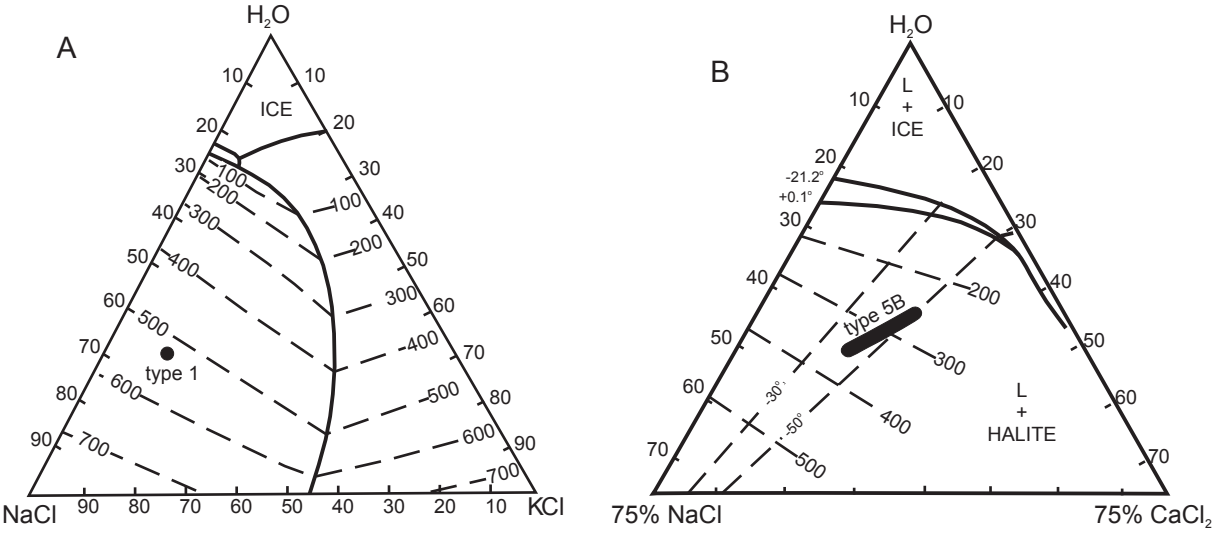

Fig. 12. Fluid inclusion data from various hydrothermal assemblages at the Malmyzh deposit. (A) NaCl-KCl-H_2O compositions of type 1 multisolid fluid inclusions in quartz from potassic alteration assemblages (phase diagram after Roedder, 1971; Sterner et al., 1988). (B) NaCl-$CaCl_2$-H_2O compositions of type 5B multisolid fluid inclusions in quartz from phyllic alteration assemblages (phase diagram after Vanko et al., 1988; Oakes et al., 1990).

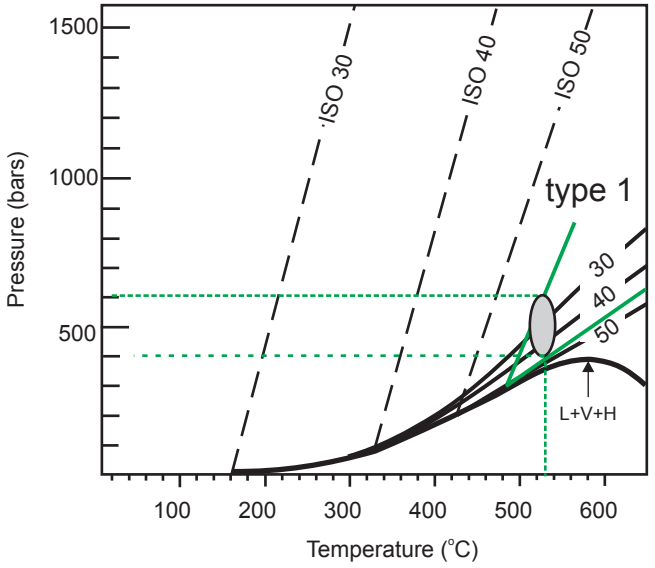

Fig. 13. Minimum pressure (shaded area) estimates for the entrapment of type 1 fluid inclusions in quartz from potassic alteration assemblages at the Malmyzh deposit. Vapor-pressure curves for H_2O-NaCl solutions and isochors are from Roedder (1984), Atkinson (2002), and Becker et al. (2008).

younger intrusive phases. Interestingly, the Nb/Zr vs. Zr diagram of Thieblemont and Tegyey (1994) indicates the presence of two groups of igneous rocks at Malmyzh: (1) the early group with subduction-related signatures, and (2) the late group with more pronounced collision-related signatures (Fig. 15A). Although the latter may have to be interpreted toward a post-subduction transform margin development of the region, rather than in favor of actual collisional environment, this is consistent with the overall transition toward the post-subduction tectonic and magmatic processes. The La/Sm vs. Sm/Yb diagram further suggests an increasing pressure of magma generation (Fig. 15B) that may be indicative of collision-related thickening of the crust (cf. Moritz et al., 2016), the latter being a common tectonic environment at many large porphyry-copper deposits (Cooke et al., 2005). By its tectonic setting affected by a strike-slip regime at a continental transform margin, the Malmyzh deposit can be compared to some other porphyry-copper deposits situated in the northern Pacific. In particular, the formation of the giant Pebble porphyry Cu-Au-Mo deposit in Alaska broadly overlapped the cessation of sedimentation and contraction and the transition to a transpressional continental margin regime, with the conversion of the remnant ocean basins to strike-slip basins (Goldfarb et al., 2013). Magmatic activity followed lithosphere thickening and an asthenospheric mantle upwelling, with subsequent post-subduction partial melting of the subcontinental lithospheric mantle and the intrusion of magma to shallow levels (Lang et al., 2013).

The Early-early Late Cretaceous tectonic regimes in the Central Sikhote-Alin differ from continent-continent collision, in some regions alternating with transform margin development (e.g., Hou and Cook, 2009; Hou et al., 2003, 2009, 2011; Ludington et al., 2012). Nevertheless, similar to the post-collisional orogens in these regions, asthenospheric mantle upwelling and injection through the slab windows (Khanchuk et al., 2016; Grebennikov et al., 2016), or lithosphere delamination, could be contributing to the overall fertility of magmas generated in the region in the Early-early Late Cretaceous. As demonstrated by Richards (2009, 2011a), re-melting of earlier subducted lithosphere comprising amphibolite cumulates and containing small amounts of sulfide minerals concentrating chalcophile and siderophile elements could produce oxidized magmas with a high water content. Hou et al. (2011) suggested a model implying partial melting of thickened or delaminated lower crust of mafic composition containing components of asthenospheric mantle, whereas productivity of the generated magma depends on copper and gold supply from the mantle and lower crust that were metasomatized during subduction and accumulation of mafic melts in the lower crust. Pirajno (2010) emphasized the role of large strike-slip fault zones in the decompression melting of the mantle material, with the generation of mafic magmas and their emplacement along the comparatively narrow conduits of the strike-slip zones; this process could be generating fertile porphyry magmas (e.g., Hou et al., 2003).

The igneous rocks at Malmyzh evolved toward water saturation that was favored by amphibole fractionation; the latter, although appears to be quite weak, is consistent with negative correlation between Dy/Yb ratios and increasing SiO_2 contents (Fig. 15C; Davidson et al., 2007; Moritz et al., 2016). The role of plagioclase fractionation was relatively minor during the 1st and 2nd intrusive stages (consistent with the lack of Eu anomalies) but significantly increased, together with biotite and K-feldspar fractionation, at the late intrusive stage, contributing to a stronger Eu minimum (Fig. 6I, 15D). As emphasized by Richards (2011b), some increase of the Sr/Y ratio approaching “adakitic” ranges,

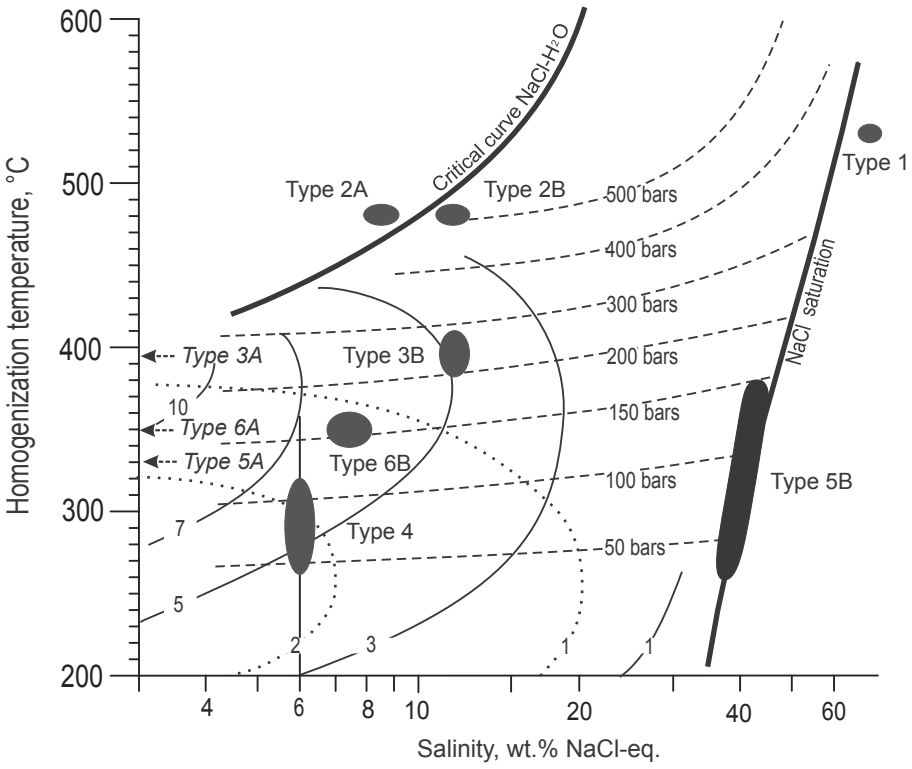

Fig. 14. Salinity-temperature diagram showing the data for type 1, 2, 3, 4, 5 and 6 fluid inclusions in quartz from potassic, propylitic and phyllic alteration assemblages at the Malmyzh deposit. Isobaric vapor pressure curves for H_2O-NaCl solutions, critical and halite saturation curves are after Roedder (1984) and Atkinson (2002). Solid and dotted lines show CO_2 solubility in H_2O-NaCl solutions under the pressure of 500 bars and 200 bars, respectively (mol.%; after Takenouchi and Kennedy, 1965).

together with the presence of hydrous phenocryst phases (amphibole, biotite), indicates increasing magmatic water content. Consistently, the dominant amphibole fractionation reflecting a high magmatic water content may have provided some "adakitic signatures" of the rocks (cf. Moritz et al., 2016). This, together with high oxidation states and elevated sulfur content, positively affects magma fertility for porphyry Cu-Au mineralization (Richards, 2011b). A distinct increase in potassium contents toward later porphyry phases may reflect an influence of deeper-seated, mantle-related magmatic sources, with a possibility of supplying volatiles (including sulfur) and metals (e.g., Cu, Au) from a deeper mafic magma chamber. A similar magmatic evolution, with subsequent emplacement of low- and then higher-K intrusive phases, was reported at many large porphyry Cu-Au deposits (e.g., McMahon, 1994; Pollard et al., 2005; Lang et al., 2013).

9.2. Elements of the tonalite-related Cu-Au ± Mo porphyry deposit model

The Malmyzh deposit is associated with a magnetite-series (Ishihara, 1981), I-type (Chappell and White, 1992) to peraluminous I-type (Chappell et al., 2012) multiphase suite of dominantly low- to medium-K calc-alkaline igneous rocks. The deposit compliments the group of large porphyry Cu-Au deposits related to low-K calc-alkaline, tonalitic magmatism and formed both in subduction-related and post-subduction settings, such as those in Indonesia (Meldrum et al., 1994), the Tethyan-Himalayan orogenic belt (e.g., Hou et al., 2003, 2011), the Andean-Cordilleran belt (e.g., Sillitoe, 1973, 2010b, 2012), the Urals (Plotinskaya et al., 2017) and other regions. Consistently, the association of Malmyzh with a dominantly low- to medium-K calc-alkaline igneous suite allows its classification toward the group of diorite- to tonalite-related porphyry Cu-Au + Mo deposits (e.g., Hollister, 1978; Holliday and Cooke, 2007). The Malmyzh deposit is characterized by an elevated Au/Cu ratio (up to 3/4), in part due to relatively minor bornite, and dominant chalcopyrite instead, and by nearly absence of Mo. The former clearly defines Malmyzh toward the group of Au-rich porphyry deposits (Sillitoe, 2000), whereas the latter differs Malmyzh from the group of porphyry Cu-Mo ± Au deposits that are associated with tonalite to plagiogranite intrusions (e.g., Yang et al., 2012; Shen et al., 2015; Pollard et al., 2017; Plotinskaya et al., 2017).

As demonstrated by Holliday and Cooke (2007), the calc-alkaline porphyry-copper systems are characterized by the intense development of a lithocap (silicic and advanced argillic alteration assemblages) that may contain a domain of high sulfidation epithermal mineralization. In contrast, alkalic porphyry-copper systems exhibit a more limited lithocap development, with the respective mineral assemblages forming dominantly along narrower steep-dipping fault zones, and are characterized by less acidic alteration assemblages (albite-sericite-K-feldspar). In this regard, the almost entire lack of advanced argillic alteration assemblages and corresponding epithermal mineralization at Malmyzh, including possible enargite-pyrite veins in the lower parts of the lithocaps (cf. Sillitoe, 2010a), is somewhat surprising, and calls for continuing efforts to locate these "missed parts" in less eroded tectonic blocks.

The calc-alkaline porphyry systems are characterized by intense development of propylitic alteration that directly envelops potassic alteration "core" and, in their "inner" zones, can overprint potassic alteration (Hollister, 1978; Holliday and Cooke, 2007). This phenomenon is clearly expressed at Malmyzh, where the "inner" propylitic assemblages and related quartz-magnetite-sulfide to quartz-sulfide veins overprint potassic alteration and bear a significant part of copper mineralization including abundant chalcopyrite and minor bornite. Disseminated copper mineralization is also associated with chlorite-quartz ± albite replacement of pervasive potassic alteration zones. Notably the "peak" of magnetite deposition is shifted toward the propylitic stage at Malmyzh, where magnetite occurs both in the form of magnetite-only, quartz-magnetite-chlorite to quartz-magnetite-sulfide veinlets and fine magnetite dissemination. The overall great abundance of magnetite has consequences for the deposit scale magnetite/pyrite ratio, which is also affected by a generally low overall pyrite content.

9.3. Magmatic-hydrothermal fluid evolution

During magmatic differentiation, magmatic melt has reached

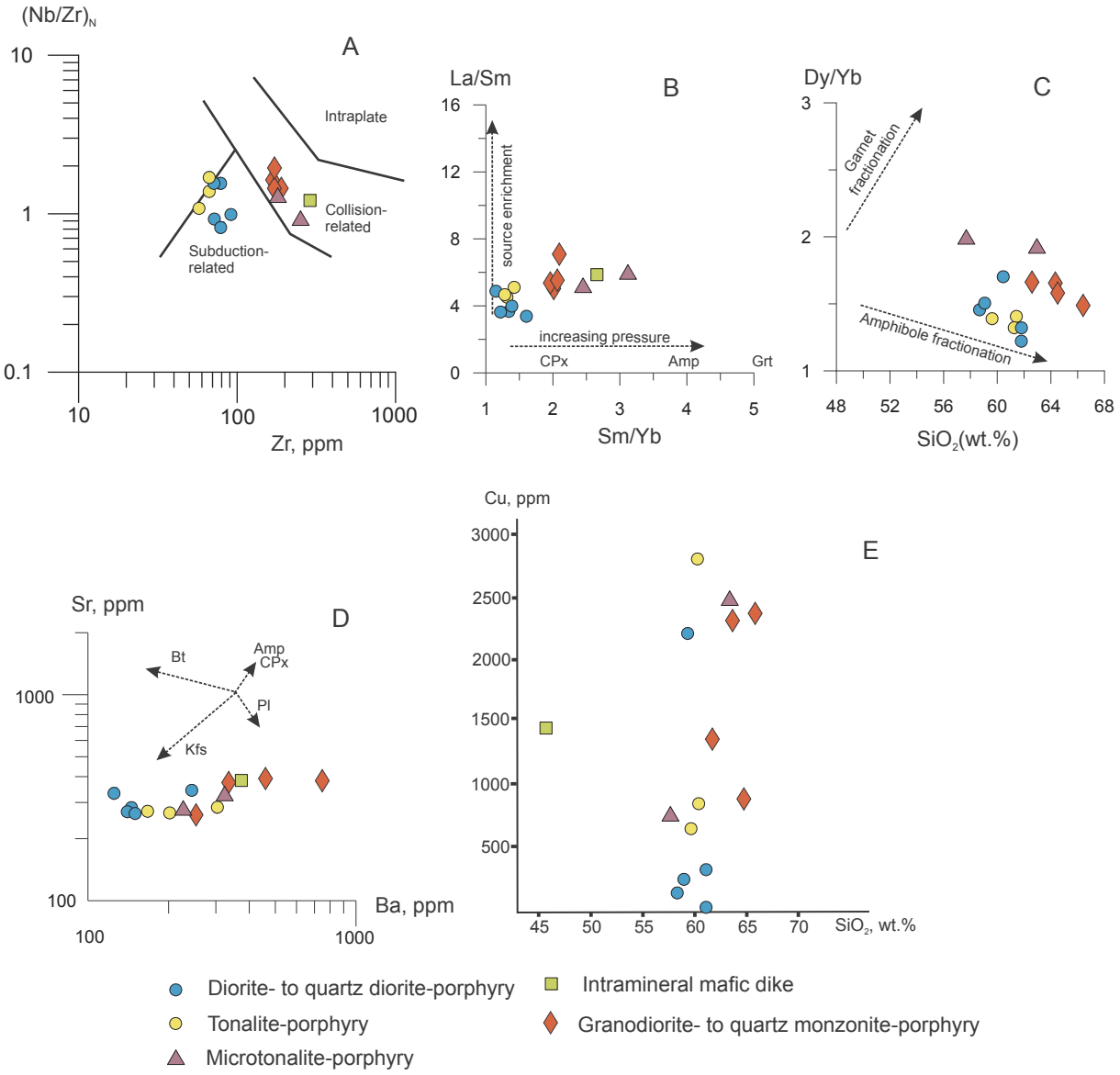

Fig. 15. Geochemical diagrams showing conditions of magma generation and evolution of igneous rocks at the Malmyzh deposit. (A) Nb/Zr vs. Zr diagram showing compositional fields of igneous rocks formed in subduction-related, collision-related and intraplate tectonic environments (Thiéblemont and Tegyey, 1994). (B) La/Sm vs. Sm/Yb diagram displaying approximate stability thresholds of clinopyroxene, amphibole and garnet stabilities in mantle melt residues (Moritz et al., 2016). (C) Dy/Yb vs. SiO_2 diagram displaying amphibole and garnet fractionation trends (Davidson et al., 2007). (D) Sr vs. Ba diagram showing dominant trends of crystallization differentiation. (E) Distribution of Cu in the igneous rocks (some values are likely affected by hydrothermal overprint). Abbreviations: CPx – clinopyroxene, Amp – amphibole, Grt – garnet, Bt – biotite, Pl – plagioclase, Ksp – K-feldspar. The individual rock compositions are from Table 2.

saturation with respect to water, at moderate (~60–65 wt%) SiO_2 content, i.e., relatively early during the magmatic evolution. Copper mineralization deposited after the intrusion of these moderately-silicic magmatic phases indicates that the magma was also saturated in copper. Sulfide saturation necessary to produce copper mineralization associated with porphyry intrusions is limited in the oxidized (magnetite-series) magma and occurs after magnetite fractionation. The latter occurring at ~60 wt% SiO_2 triggers sulfide saturation due to the conversion of most of the sulfur originally dissolved in the magma as sulfate, with the Cu-rich sulfide phase represented by bornite sequestering gold (Jenner et al., 2010). Sun et al. (2015) emphasized that the oxidized magma remains sulfide-undersaturated during the early stages of its evolution; sulfide saturation occurs and the metals are partitioned into coexisting magmatic-hydrothermal fluids following reduction accompanying magnetite crystallization. Consistently, the copper distribution in the igneous rocks at Malmyzh shows a tendency of enrichment toward the later intrusive stages (Fig. 15E), although a caution should be exercised due to the possible hydrothermal overprint effect.

The high content of volatiles in the magma, among other features, is supported by the abundance of the dikelets (microdikes, or "veindikes") at Malmyzh. These narrow (1–2 mm to 1–2 cm) dikelets, which locally form a dense network, couldn't be emplaced without being saturated in volatiles preventing a rapid crystallization; consistently, they provide a link between magmatic and hydrothermal processes (Seedorff et al., 2005). The presence of chalcopyrite in their core parts also indicates a saturation of the transitional magmatic-hydrothermal fluid in copper. Intense multiple magmatic brecciation, with large intrusive (eruptive) breccia bodies, further support a high content of volatiles. Magma emplacement at shallow (porphyry) levels promoted direct exsolution of metalliferous high-salinity aqueous fluids from crystallizing volatile-rich intrusions (Cline and Bodnar, 1994; Bodnar, 1995;

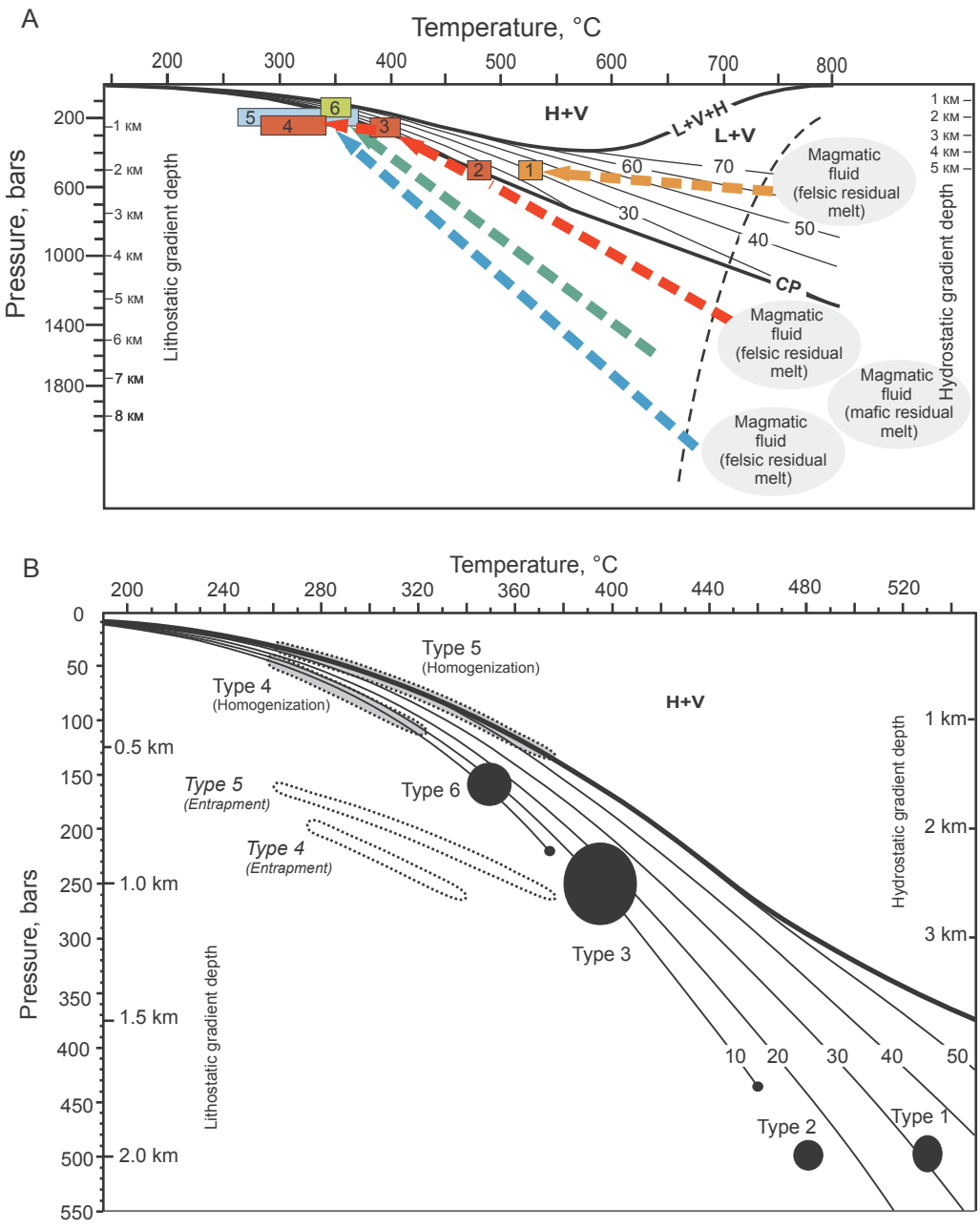

Fig. 16. Estimated pressure and temperature conditions and evolutional paths for different fluid inclusion types in hydrothermal assemblages at the Malmyzh deposit (A) and part of thus diagram for low P and T conditions (B), with composition of different fluid inclusion types as a function of depth and temperature in relation to various intrusive phases (the principal diagram after Bodnar et al., 1985; Fournier, 1999). Vapor pressure curves for H_2O-NaCl solutions at 0–70 wt% NaCl and the three-phase (L + V + H) curve are shown after Atkinson (2002) and Becker et al. (2008). Dashed line represents water-saturated granite solidus (Holtz et al., 2001). PT-fields for the major fluid inclusion types and possible evolutional paths for fluids (arrows) are shown.

Shinohara and Hedenquist, 1997; Harris et al., 2004; Audetat et al., 2008). This is consistent with the presence of high-salinity type 1 fluid inclusions in potassic alteration assemblages at Malmyzh that are homogenized by halite dissolution (cf. Cline and Bodnar, 1994; Bodnar, 1995). The fluid inclusion data (Table 4) indicate the formation of potassic alteration assemblages from a homogenous hot (~525–530 °C, up to 550 ± 5 °C), high-salinity (57–58 wt% NaCl and 13–12 wt% KCl), dominantly sodic-potassic aqueous-chloride fluid (type 1 fluid inclusions), at the pressures of 500 ± 100 bars corresponding to a lithostatic depth of ~2 km (Fig. 16).

Further magmatic intrusion and crystallization was accompanied by separation of a magmatic-hydrothermal fluid, with its further cooling and/or its ascent to shallower levels causing fluid phase separation. Consistently, the early quartz-magnetite ± chlorite (M − type) veinlets in zones of propylitic alteration contain an assemblage of gaseous lower-salinity (type 2A) and higher-salinity (type 2B) fluid inclusions homogenizing at ~ 480 ± 5 °C and indicating fluid boiling. However, due to near-critical conditions of the phase separation into coexisting lower- (8–9 wt% NaCl-eq.) and higher-salinity fluids (11–12 wt% NaCl-eq.), this process resulted in the both the separating and original fluids exhibiting minor differences in salinity.

The subsequent most productive Cu-Au mineralization appears to occur during two different and compositionally distinct, although similar (overlapping) in the PT-conditions, mineralizing events. First, at the propylitic alteration stage, quartz-sulfide-magnetite to quartz-sulfide veinlets cutting the laminated quartz-magnetite veinlets were initially formed from a boiling magmatic-hydrothermal aqueous fluid during its cooling and/or ascent to shallower levels (cf. Hedenquist et al., 1998), with corresponding separation into a low-salinity vapor and coexisting higher-salinity fluid (11–12 wt% NaCl-eq.) at the temperatures of 410–380 °C (type 3A and 3B fluid inclusions; Table 4). A younger FIA in these veinlets comprises liquid-gaseous type 4 fluid inclusions that homogenize at the temperatures of 320–260 °C and indicate a homogenous aqueous-chloride fluid (Table 4). Dominant NaCl and KCl characterized the mineralizing fluid during propylitic alteration.

Second, at the phyllic alteration stage, early quartz-sericite and quartz-sericite-carbonate veinlets with chalcopyrite cutting zones of pervasive potassic alteration contain an assemblage of gaseous (type 5A) and high-salinity (type 5B) fluid inclusions indicating fluid boiling. Homogenization of these fluid inclusions occurs over a broad range of temperatures (from 380 to 250 °C) essentially overlapping these during the preceding propylitic stage (Fig. 16). These conditions correspond to continuing deposition of Cu and Au minerals in zones of quartz-sericite replacement of chlorite-dominant mineral assemblages of the preceding propylitic stage, with the formation of the composite quartz-chlorite-sericite aggregate. Consistently, the phyllic alteration stage can correspond to another cycle of fluid exsolution from crystallizing magma, possibly representing a younger intrusive phase (Fig. 16; cf. Harris and Golding, 2002), including that with a greater degree of differentiation (cf. Mustard et al., 2006). A new fluid source, as compared to the preceding propylitic stage, is also supported by a different (dominantly sodic-calcic) fluid composition (Table 4). Further cooling of this fluid and/or its ascent to shallower levels could cause phase separation into a low-salinity vapor and coexisting brine (from 34 wt% NaCl and 16 wt% $CaCl_2$ to 22 wt% NaCl and 23 wt% $CaCl_2$) (cf. Hedenquist et al., 1998). The late quartz-pyrite ± sericite veins and pervasive pyrite-rich silicification zones assigned to the phyllic alteration stage were also formed from a boiling, although NaCl + KCl-dominant, fluid (type 6A and 6B fluid inclusions).

The presence of opaque solid phase(s), likely chalcopyrite, in the type 5A fluid inclusions indicates a high metal endowment of the magmatic-hydrothermal fluid. This also suggest a possibility that some metals (including Cu and Au) were partitioned into gaseous phase (Ulrich et al., 1999; Audetat et al., 2008; Williams-Jones and Heinrich, 2008). Furthermore, this can manifest a porphyry-epithermal transition, with an acidic gaseous fluid ascending to shallower levels and transporting copper and other metals in epithermal environment (cf. Arribas, 1995; White and Hedenquist, 1995; Hedenquist et al., 1998; Simmons et al., 2005; Kouzmanov and Pokrovski, 2012; Corbett, 2017).

The presence of Te, Bi, Sb, Hg mineralization in phyllic alteration assemblages suggests a possible fluid supply from a mafic residual magmatic melt, mantle-related mafic magma, or from a mixed mafic and granitoid source that would be feasible during a multistage magmatic evolution (Fig. 16). A possibility of supplying of fluids and metals (e.g., Cu, Au) from a mafic magma chamber was reported at many porphyry Cu-Au and Cu-Au-Mo deposits (e.g., Keith et al., 1998; Hattori and Keith, 2001; Maughan et al., 2002; Pollard et al., 2005; Redmond and Einaudi, 2010; Muller and Groves, 2019).

9.4. Timing of copper and gold deposition

Copper mineralization at Malmyzh is present in most of mineral assemblages of the potassic and propylitic alteration stages and, to a lesser extent, in the assemblages of the phyllic alteration stage. However, the “peak” of copper mineralization, principally in the form of chalcopyrite, with typically minor bornite (at least at the deposit level studied), begins with a later event during the propylitic alteration stage, particularly with quartz-sulfide-magnetite and quartz-sulfide veins and related sulfide dissemination. These veins post-date chlorite-magnetite, magnetite and quartz-magnetite veins formed during an early event of the propylitic alteration stage. The most intense Cu-Au deposition continued also during sericite (quartz-sericite) replacement of chlorite, i.e. the process assigned to the beginning of the next, phyllic alteration stage. In contrast, further development of phyllic alteration, with abundant quartz and pyrite, causes removal of copper minerals.

Gold mineralization is represented by at least three generations: the early native gold (fineness 980‰) is associated with magnetite and bornite of the propylitic stage; the intermediate native gold (fineness 850–760‰) and electrum (fineness 511–616‰) occur in chalcopyrite; and the late native gold (fineness ~ 925‰) is associated with telluride minerals formed during the phyllic alteration stage. Consistently, the gold deposition at Malmyzh was likely a long-lasting process, corresponding to the propylitic and phyllic alteration stages. Tellurium mineralization was formed during the phyllic alteration stage over a large temperature interval (cf. Afifi et al., 1988; Zhang and Spry, 1994; Bogdanov et al., 2005; Mueller and Muhling, 2020). Part of the gold-telluride mineralization may represent a porphyry-epithermal transition (e.g., Zhang and Spry, 1994).

The relatively low-temperatures (~380 °C to 260 °C) of the dominant Cu and Au deposition corresponding to the end of the propylitic and the beginning of the phyllic alteration stages differ Malmyzh from many porphyry Cu-Au deposits, where Cu and Au are precipitated mainly at the potassic alteration stage (e.g., Lowell and Guilbert, 1970; Seedorff et al., 2005; Sillitoe, 2010a). However, similar to Malmyzh, Cu and Au are paragenetically late at many other porphyry Cu-Au deposits (Pirajno, 2009), where the main Cu-ore deposition occurred in the porphyry environment at lower temperatures, in the order of 350–300 °C and slightly lower (e.g., Hedenquist et al., 1998; Harris and Golding, 2002; Harris et al., 2004; Seedorff et al., 2005; Rusk et al., 2008; Klemm et al., 2007; Gregory, 2017; Tsuruoka, 2017). Consistently, this leads to another model, where Cu-Au mineralization is related to propylitic and early phyllic alteration events, which overprint potassic alteration. The relatively lower-temperature process of copper deposition corresponds to chalcopyrite precipitation below 400 °C due to a drop in its temperature-dependent solubility and the generation of H_2S by disproportionation of SO_2 upon cooling (Landtwing et al., 2005; Hezarkhani et al., 1999). Fluid boiling also favored metal deposition (Drummond and Ohmoto, 1985). An environment of lower fO_2 and elevated fS_2 resulting in destruction of most magnetite and its substitution by pyrite favored Au deposition from magmatic-hydrothermal fluid at lower temperatures, as partitioning of Au in this process is essentially influenced by the behavior of sulfur, with lower fO_2 facilitating sulfide (bearing Au) precipitation from mineralized fluids (e.g., Yang, 2012).

10. Conclusions

The Malmyzh deposit is a large porphyry Cu-Au deposit and the largest porphyry Cu-Au deposit cluster in eastern Russia. It is located in a turbidite terrane, and was formed under a transform continental margin regime. The deposit is related to a magnetite-series, dominantly low-K calc-alkaline diorite-tonalite igneous suite, with a higher K content in the younger intrusion phases. The magma was emplaced in a series of separated local magmatic centres (“porphyry centres”) that vary in petrologic features and relative abundance of different igneous rocks as well as in the dominant development of different hydrothermal alteration and mineralization types. In total, the deposit may represent part of a new large (region-scale) province of porphyry Cu-Au ± Mo deposits related to the Early-early Late Cretaceous magmatism in the Sikhote-Alin orogenic belt. The parental igneous suite at Malmyzh was coeval to ilmenite-series calc-alkaline granitoid suites, which are accompanied by reduced intrusion-related Au(± W) to W-Au deposits.

The deposit comprises intense quartz-K-feldspar ± biotite ± chalcopyrite stockworks in zones of potassic alteration, followed by quartz-magnetite and then by quartz-sulfide-magnetite (with chalcopyrite and bornite) stockworks in zones of propylitic alteration. The mineralized stockworks are partially overprinted by quartz-sericite and quartz-pyrite stockworks formed during phyllic alteration stage. The most productive copper mineralization is related to a later hydrothermal event during the propylitic alteration stage, and to an early event during the phyllic alteration stage, the latter manifested by chlorite replacement by sericite. Further development of phyllic alteration, however, caused a dilution of copper grades. Three generations of gold are distinguished, including the early generations associated with magnetite and bornite of the propylitic stage, intermediate generation associated with chalcopyrite, and the late generation associated with pyrite of the phyllic stage. Overall, the deposit corresponds

to the "diorite model" of Cu-Au porphyry deposits, with elevated Au/Cu ratio and very minor Mo, intense development of propylitic alteration assemblages overprinting potassic alteration and causing abundant magnetite and copper sulfide deposition, and with a relatively low pyrite content in propylitic and phyllic alteration assemblages. Part of gold mineralization precipitated in the form of Au and Au-Ag tellurides and/or in association with Bi-Te minerals.

Potassic alteration assemblages formed from a homogenous high-salinity (57–78 wt% NaCl and 13–12 wt% KCl), high-temperature (> 525–535 °C), sodic-potassic aqueous-chloride fluid, with its possible direct separation from crystallizing magma under the pressure of 500 ± 100 bars. At the propylitic stage, the early quartz-magnetite-chlorite assemblage was formed from a lower temperature (480 ± 5 °C), sodic-dominant aqueous-chloride fluid, under near-critical conditions and a similar pressure (~500 bars). As the magma degassing progressed, late (quartz-sulfide-magnetite) propylitic alteration assemblages formed initially from a boiling fluid at 410–380 °C and then from a cooling (320–260 °C) homogenous sodic-potassic-dominant, aqueous-chloride fluid. Phyllic alteration assemblages formed due to another cycle of fluid exsolution from crystallizing magma, possibly representing a younger intrusive phase, from a boiling and cooling (from ~ 380 to 250 °C), sodic-calcic to calcic-sodic aqueous-chloride fluid, with its subsequent boiling and separation into gaseous and high-salinity (from 34 wt% NaCl and 16 wt% $CaCl_2$ to 22 wt% NaCl and 23 wt% $CaCl_2$) aqueous-chloride phases. Consistently, the temperatures of ~ 380 °C to 260 °C during the propylitic and phyllic alteration stages correspond to the most intense Cu and Au mineralization at Malmyzh.

Acknowledgments

This paper represents part of the authors' work on research and assessment of porphyry Cu-Au deposits in eastern Russia. The authors thank Olga Artemova and Pavel Selivanov for their helpful participation in drill core logging and sampling. The authors are grateful to Vasily Shapovalenko, Alexander Efimov, Evgeny Ignatiev, Andrey Chitalin and Vladislav Mramornov for fruitful discussions. Tom Bowens provided logistic support and access to the drill core. Vladimir Vakhrushev and Maxim Kremenetsky (Russian Copper Company) are thanked for the permission to publish the data. The work was financially supported by the Program no. 72-4 of the Russian Academy of Sciences and the Scientific Program of IGEM RAS, and by the Contract no. 049-00015-19-00 of TsNIGRI. Editorial reviews by Franco Pirajno, Alexander Yakubchuk and two anonymous reviewers significantly improved the paper.

Appendix A. Supplementary data

Supplementary data to this article can be found online at https://doi.org/10.1016/j.oregeorev.2019.103112.

References

Afifi, A.M., Kelly, W.C., Essene, E.J., 1988. Phase relations among tellurides, sulfides, and oxides: II. Applications to telluride-bearing ore deposits. Econ. Geology 83, 395–404.

Arribas Jr., A., 1995. Characteristics of high-sulfidation epithermal deposits, and their relation to magmatic fluid. Miner. Assoc. Canada Short Course 23, 419–454.

Atkinson, A.B., 2002. A model for the PTX properties of H_2O-NaCl. M.Sc.Thesis. Virginia Tech. Institute and State University, pp. 126.

Audetat, A., Pettke, T., Heinrich, C.A., Bodnar, R.J., 2008. The composition of magmatic-hydrothermal fluids in barren and mineralized intrusions. Econ. Geology 103, 877–908.

Becker, S.P., Fall, A., Bodnar, R.J., 2008. Synthetic fluid inclusions. XVII. PVTX properties of high-salinity H_2O-NaCl solutions (> 30 wt.% NaCl): applications to fluid inclusions that homogenize by halite disappearance from porphyry copper and other hydrothermal ore deposits. Econ. Geol. 103, 539–544.

Belyansky, G.S., Rybalko, V.I., Syasko, A.A., Bazhanov, V.A., Uglova, N.I., Abramova, V.A., Oleinikov, A.B., Kovalenko, S.V., Kashtaev, B.I., Alenicheva, A.A., Gonokhova, N.G., 2011. Explanatory notes to the geological map of Russia, L-52/53, and K-52/53 map sheets, 1: 1,000,000 scale, 3rd generation. VSEGEI, St-Petersburg. 699 (in Russian).

Bodnar R.J., 1995. Fluid inclusion evidence for a magmatic source for metals in porphyry copper deposits. In: Thompson, J.F.H. (ed.): Magmas, fluids, and ore deposits. Min. Assoc. Canada Short Course Series 23, 139-152.

Bodnar, R.J., Burnham, C.W., Sterner, S.M., 1985. Synthetic fluid inclusions in natural quartz. III. Determination of phase equilibrium properties in the system H_2O-NaCl to 1000°C and 1500 bars. Geochim. Cosmochim. Acta 49, 1861–1873.

Bodnar, R.J., Vityk, M.O., 1994. Interpretation of microthermometric data for H_2O-NaCl fluid inclusions. In: De Vivo, B., Frezzotti, M.L. (Eds.), Fluid inclusions in minerals, methods and applications. Blacksburg, Virginia Tech, pp. 117–130.

Bogdanov, K., Filipov, A., Kehayov, R., 2005. Au-Ag-Te-Se minerals in the Elatsite porphyry-copper deposit, Bulgaria. Geochem., Mineral Petrol. 43, 13–19.

Bukhanova D.S., 2018. First data on the age of the Malmyzh copper-gold porphyry deposit, Khabarovsk Region. In: Petrov V.A., Amplieva E.E., Ustinov S.A., Kovalchuk E. V. (eds.), New Data in the Understanding of the Mineral Formation Processes, 8th Youth Scientific-Practical School, 26-30 Nov. 2018, Moscow, IGEM RAS, pp. 81-82 (in Russian).

Bukhanova, D.S., Plechov, P.Y., 2017. Conditions of formation of the Malmyzh Cu-Au porphyry deposit, Khabarovsk Region (as revealed by fluid inclusion study). Proc. KRAUSC, Earth Sciences 34 (2), 61–71 (in Russian).

Canby V.M., 2019. Bootprints in bear country: geology and discovery history of the Malmyzh Cu-Au porphyry deposits, Khabarovsk Krai, Russia. Denver Region Exploration Geologists' Society, Abstracts, Feb. 2019. http://www.dregs.org/abs2019.html.

Chappell, B.W., Bryant, C.J., Wyborn, D., 2012. Peraluminous I-type granites. Lithos 153, 142–153.

Chappell, B.W., White, A.J.R., 1992. I- and S-type granites in the Lachlan Fold Belt. Trans. Royal Soc Edinburgh, Earth Sci. 83, 1–26.

Chernyavsky, V.S., Shavkunov, N.A., 1976. Report on prospecting for gold on the Malmyzh and Bolon Heights, Khomi, Kargi and Jubileinoe Zones (Malmyzh Team) for 1974–1976. Khabarovsk, USSR Ministry of Geology 156 (in Russian).

Chernyavsky, V.S., Sokolov, N.A., 2015. Report on the results of prospecting for ore gold in the Poniy-Mulin ore-placer cluster in the Khabarovsk Region for 2013–2015 (map sheet M-43-XVIII). Khabarovsk, Dalgeophysica JSV 729 (in Russian).

Chitalin, A.F., Efimov, A.A., Voskresensky, K.I., Ignatiev, E.K., Kolesnikov, A.G., 2013. Malmyzh – new large copper-gold porphyry system of the world class in the Sikhote-Alin. Mineral Resources of Russia, Economics and Management 3, 65–69 (in Russian).

Chitalin, A., Shtengelov, A., Agapitov, D., Fomichev, E., Usenko, V., Matevosyan, M., 2011. Geology and mineral resources of the giant Peschanka porphyry Cu-Au-Mo deposit, Western Chukotka, Russia, Proc. 11th SGA Biennial Meeting, 2011, Chile, Antofagasta: Univ. Catolica Norte, pp. 263–264.

Clark, A.H., 1993. Are outsized porphyry copper deposits either anatomically or environmentally distinctive? Soc. Econ. Geol. Spec. Publ. 2, 213–283.

Cline, J.S., Bodnar, R.J., 1994. Direct evolution of brine from a crystallizing silicic melt at the Questa, New Mexico, molybdenum deposit. Econ. Geology 89, 1780–1802.

Cooke, D.R., Hollings, P., Walshe, J.L., 2005. Giant porphyry copper deposits: characteristics, distribution, and tectonic controls. Econ. Geol. 100, 801–818.

Corbett. G.J., 2017. Epithermal Au-Ag and porphyry Cu-Au exploration. Short Course Manual, Sept. 2017 edition. www.corbettgeology.com.

Corbett, G.J., Leach, T.M., 1998. Southwest Pacific Rim gold-copper systems: Structure, alteration and mineralization. SEG Spec. Publ. 6, 238 p.

Crawford M.L., 1981. Phase equilibria in aqueous fluid inclusions. In: Hollister L.S., Crawford M.L. (Eds) Fluid inclusions: Application to Petrology. Min Assoc Canada Short Course Handbook, Calgary 6, pp. 75-100.

Davidson, J., Turner, S., Handley, H., Macpherson, C., Dosseto, A., 2007. Amphibole "sponge" in arc crust? Geology 35, 787–790.

Defant, M.J., Drummond, M.S., 1990. Derivation of some modern arc magmas by melting of young subducted lithosphere. Nature 347, 662–665.

Drummond, S.E., Ohmoto, H., 1985. Chemical evolution and mineral deposition in boiling hydrothermal systems. Econ. Geology 80, 126–147.

Fournier, R.O., 1999. Hydrothermal process related to movement of fluid from plastic into brittle rock in the magmatic-epithermal environment. Econ. Geol. 94, 1193–1212.

Garwin, S., Hall, R., Watanabe, Y., 2005. Tectonic setting, geology, and gold and copper mineralization in Cenozoic magmatic arcs of southeast Asia and the west Pacific. Econ. Geology, 100th Anniv. Vol. 891–930.

Goldfarb, R.J., Anderson, E.D., Hart, C.J.R., 2013. Tectonic setting of the Pebble and other copper-gold molybdenum porphyry deposits within the evolving middle Cretaceous continental margin of northwestern North America. Econ. Geol. 108, 405–419.

Goldstein, Robert H., Reynolds, T. James (Eds.), 1994. Systematics of Fluid Inclusions in Diagenetic Minerals. SEPM (Society for Sedimentary Geology).

Gonevchuk, V.G., Gonevchuk, G.A., Korostelev, P.G., Semenyak, B.I., Seltmann, R., 2010. Tin deposits of the Sikhote-Alin and adjacent areas (Russian Far East) and their magmatic association. Australian J. Earth Sci. 57 (6), 777–802.

Grebennikov, A.V., Khanchuk, A.I., Gonevchuk, V.G., Kovalenko, S.V., 2016. Cretaceous and Paleogene granitoid suites of the Sikhote-Alin area (Far East Russia): geochemistry and tectonic implications. Lithos 261, 250–261.

Gregory, M.J., 2017. A fluid inclusion and stable isotope study of the Pebble porphyry copper-gold-molybdenum deposit, Alaska. Ore Geology Rev. 80, 1279–1303.

Gustafson, L.B., Hunt, J.P., 1975. The porphyry copper deposit at El Salvador, Chile. Econ. Geology 70, 857–912.

Gvozdev, V.I., Dobroshevskii, K.N., Vakh, A.S., Goryachev, N.A., Stepanov, V.A., Fedoseev, D.G., 2016. The Malinovskoe deposit as a new type of gold mineralization in the Primorie region, Russia (geology, mineralization, and genesis). Pacific Geology 35 (1), 37–53 (in Russian).

Harris, A.C., Golding, S.D., 2002. New evidence of magmatic-fluid-related phyllic

alteration: implications for the genesis of porphyry Cu deposits. Geology 30, 335–338.
Harris, A.C., Kamenetsky, V.S., White, N.C., Steele, D.A., 2004. Volatile phase separation in silicic magmas at Bajo de la Alumbrera porphyry Cu-Au deposit, NW Argentina. Resour. Geol. 54, 341–356.
Hart C.J.R., 2007. Reduced intrusion-related gold systems. In Goodfellow W.D. (ed.), Mineral Deposits of Canada: A Synthesis of Major Deposit Types, District Metallogeny, the Evolution of Geological Provinces, and Exploration Methods. Geological Association of Canada, Mineral Deposits Division, Special Publication no. 5, p. 95-112.
Hattori, K.H., Keith, J.D., 2001. Contribution of mafic melt to porphyry copper mineralization: Evidence from Mount Pinatubo, Philippines, and Bingham Canyon, Utah, USA. Miner. Deposita 36, 799–806.
Hedenquist, J.W., Arribas, A., Reynolds, T.J., 1998. Evolution of an intrusion-centered hydrothermal system: Far Southeast-Lepanto porphyry and epithermal Cu-Au deposits. Philippines. Econ. Geology 93, 373–404.
Hezarkhani, A., Williams-Jones, A.E., Gammons, C.H., 1999. Factors controlling copper solubility and chalcopyrite deposition in the Sungun porphyry copper deposit. Iran. Miner. Deposita. 34, 770–783.
Holliday J.R., Cooke D.R., 2007. Advances in geological models and exploration methods for copper ± gold porphyry deposits. In: Milkereit D. (ed.), Proceedings of Exploration 2007: Fifth Internat.Conf. Min. Exploration, pp. 791-809.
Holliday, J.R., Wilson, A.J., Blevin, P.L., Tedder, I.J., Dunham, P.D., Pfitzner, M., 2002. Porphyry gold-copper mineralization in the Cadia district, eastern Lachlan fold belt, New South Wales, and its relationship to shoshonitic magmatism. Miner. Deposita 37, 100–116.
Hollister, V.F., 1978. Geology of Porphyry Copper Deposits of the Western Hemisphere. Society of Mining Engineering, AIME, New York, pp. 219.
Holtz, F., Becker, A., Freise, M., Johannes, W., 2001. The water-undersaturated and dry Qz-Ab-Or system revisited. Experimental results at very low water activities and geological implications. Contrib. Mineral. Petrol. 141, 347–357.
Hou, Z., Cook, N.J., 2009. Metallogenesis of the Tibetan collisional orogen: a review and introduction to the special issue. Ore Geology Reviews 36, 2–24.
Hou, Z., Yang, Z., Qu, X., Meng, X., Li, Z., Beaudoin, G., Rui, Z., Gao, Y., Zaw, K., 2009. The Miocene Gangdese porphyry copper belt generated during post-collisional extension in the Tibetan Orogen. Ore Geol. Rev. 36, 25–51.
Hou, Z., Zhang, H., Pan, X., Yang, Z., 2011. Porphyry (Cu-Mo-Au) deposits related to melting of thickened mafic lower crust - examples from the eastern Tethyan metallogenic domain. Ore Geology Rev. 39, 21–45.
Hou, Z., Ma, H., Zaw, K., Zhang, Y., Wang, M., Wang, Z., Pan, G., Tang, R., 2003. Himalayan Yulong porphyry copper belt - product of large-scale strike-slip faulting in eastern Tibet. Econ. Geology 98, 125–145.
Ishihara, S., 1981. The granitoid series and mineralization. Econ. Geology 75, 458–484.
Ivin, V.V., Rodionov, A.N., Medvedev, E.I., Fatyanov, I.I., 2017. Peculiarities of location of various precious mineralization in the Primorie region and its resource potential. Adv. Curr. Nat. Sci. Earth Sci. 8, 80–89 (in Russian).
Jahn, B.M., Valui, G., Kruk, N., Gonevchuk, V., Masako, U., Wu, J.T.J., 2015. Emplacement ages, geochemical, and Sr-Nd-Hf isotopic characterization of Mesozoic to Early Cenozoic granitoids of the Sikhote-Alin orogenic belt, Russian Far East: crustal growth and regional tectonic evolution. J. Asian Earth Sci. 111, 872–918.
Jenner, F.E., O'Neil, H.S.C., Arculus, R.J., Mavrogenes, J.A., 2010. The magnetite crisis in the evolution of arc-related magmas and the initial concentration of Au, Ag and Cu. Jour. Petrol. 51, 2245–2264.
Keith J.D., Christiansen E.H., Maughan D.T., Waite K.A., 1998. The role of mafic alkaline magmas in felsic porphyry Cu and Mo systems. In: Lentz D.R. (Ed.), Mineralized intrusion-related skarn systems: Miner Assoc Canada Short Course 26, pp. 211-243.
Khanchuk, A.I., Golozubov, V.V., Martinov, Yu.A., Simanenko, V.P., 1997. The Early Cretaceous and Paleogene transform continental margins (Californian type) of the Russian Far East. In: Tectonics of Asia. Moscow, GEOS Publishing, pp. 240-243 (in Russian).
Khanchuk A.I., Gonevchuk V.G., Bortnikov N.S., Gorelikova N.V., 2003. Paleogeodynamic model of Sikhote-Alin tin-bearing system (Russia). In: Mineral exploration and sustainable development: Proceedings of the 7th Biennial SGA Meeting, vol. 1. Millpress, Rotterdam. pp. 295-298.
Khanchuk, A.I., Kemkin, I.V., Kruk, N.N., 2016. The Sikhote-Alin orogenic belt, Russian South East: terranes and the formation of continental lithosphere based on geological and isotopic data. J. Asian Earth Sci. 120, 117–138.
Klemm, L.M., Pettke, T., Heinrich, C.A., Campos, E., 2007. Hydrothermal evolution of the El Teniente deposit, Chile: Porphyry Cu-Mo ore deposition from low-salinity magmatic fluids. Econ. Geology 102, 1021–1045.
Kouzmanov K., Pokrovski, G.S., 2012. Hydrothermal controls on metal distribution in porphyry Cu (-Mo-Au) systems. In: Hedenquist J.W., Harris M., Camus F. (eds.), Geology and Genesis of Major Copper Deposits and Districts of the World: A Tribute to Richard H. Sillitoe. SEG Spec. Publ. 16, pp. 573–618.
Kruk, N.N., Simanenko, V.P., Gvozdev, V.I., Golozubov, V.V., Kovach, V.P., Serov, P.A., Moskalenko, E.Yu., Kuibida, M.L., 2014. Geochemical characteristics and sources of the melts of the Early Cretaceous granitoids in the Samarga terrain (Sikhote-Alin). Russian Geol. Geophys. 2, 276–302.
Landtwing, M.R., Pettke, T., Halter, W.E., Heinrich, C.A., Redmond, P.B., Einaudi, M.T., Kunze, K., 2005. Copper deposition during quartz dissolution by cooling magmatic-hydrothermal fluids: The Bingham porphyry. Earth Planet. Sci. Letters 235, 229–243.
Lang, J.R., Gregory, M.J., Rebagliati, C.M., Payne, J.G., Oliver, J.L., Roberts, K., 2013. Geology and magmatic-hydrothermal evolution of the giant Pebble porphyry copper-gold-molybdenum deposit, southwest Alaska. Econ. Geology 108, 437–462.
Lang, J.R., Stanley, C.R., Thompson, J.F.H., 1995. Porphyry copper-gold deposits related to alkalic igneous rocks in the Triassic-Jurassic arc terranes of British Columbia. Arizona Geological Society Digest 20, 219–236.
Le Maitre, R.W., Bateman, P., Dudek, A., Keller, J., Lameyre, J., Le Bas, M.J., Sabine, P.A., Schmid, R., Sorensen, H., Streckeisen, A., Wooley, A.R., Zanettin, B., 1989. A classification of igneous rocks and glossary of terms. Blackwell, Oxford, pp. 193.
Lowell, J.D., Guilbert, J.M., 1970. Lateral and vertical alteration-mineralization zoning in porphyry ore deposits. Econ. Geology 65, 373–408.
Ludington, S., Hammarstrom, J.M., Robinson Jr., G.R., Mars, J.C., Miller, R.J., 2012. Porphyry copper assessment of the Tibetan Plateau, China. U.S. Geological Survey Scientific Investigations Report 2010–5090-F, 63.
MacLean, W.H., Barrett, T.J., 1993. Lithogeochemical techniques using immobile elements. J. Geochem. Explor. 48, 109–133.
Malinovsky, A.I., 2011. Lithochemical composition of terrigenous rocks of the Zhuravlevka terrane (Sikhote-Alin) and its geodynamic interpretation. Proc. KRASRC 18 (2), 14–30 (in Russian).
Malinovsky, A.I., Golozubov, V.V., 2012. Structure, composition and formation environments of Lower Cretaceous sediments of the Zhuravlevka terrane (Central Sikhote-Alin). Lithology and Mineral Deposits 4, 399–424 (in Russian).
Maniar, P.D., Piccoli, P.M., 1989. Tectonic discrimination of granitoids. Geol. Soc. Amer Bull 101, 635–643.
Martin, H., Smithies, R.H., Rapp, R., Moyend, J.F., Champion, D., 2005. An overview of adakite, tonalite–trondhjemite–granodiorite (TTG), and sanukitoid: relationships and some implications for crustal evolution. Lithos 79, 1–24.
Maughan, D.T., Keith, J.D., Christiansen, E.H., Pulsipher, T., Hattori, K., Evans, N.J., 2002. Contributions from mafic alkaline magmas to the Bingham porphyry Cu-Au-Mo deposit, Utah, USA. Miner. Deposita 37, 14–37.
Masterman, G.J., Cooke, D.R., Berry, R.F., Walshe, J.L., Lee, A.W., Clark, A.H., 2005. Fluid chemistry, structural setting, and emplacement history of the Rosario Cu-Mo porphyry and Cu-Ag-Au epithermal veins, Collahuasi District, Northern Chile. Econ. Geol. 100, 835–862.
McDonough, W.F., Sun, S.-S., 1995. The composition of the Earth. Chemical Geology 120, 223–253.
McMahon, T.P., 1994. Pliocene intrusions in the Gunung Bijih (Ertsberg) mining district, Irian Jaya, Indonesia: major- and trace-element chemistry. Internat. Geology Rev. 36, 925–946.
Meldrum, S.J., Aquino, R.S., Gozales, R.I., Burke, R.J., Suyadi, A., Irianto, B., Clarke, D.S., 1994. The Batu Hijau porphyry copper-gold deposit, Sumbawa Island. Indonesia. Jour. Geochem. Explor. 50, 203–220.
Middlemost, E.A.K., 1997. Magmas. Rocks and Planetary Development, Longman, Harlow, pp. 299.
Mihalasky, M.J., Ludington, S., Alexeiev, D.V., Frost, T.P., Light, T.D., Briggs, D.A., Hammarstrom, J.M., Wallis, J.C., Bookstrom, A.A., Panteleyev, A., 2015. Porphyry copper assessment of northeast Asia-Far East Russia and Northeasternmost China. U.S. Geological Survey Scientific Investigations Report 2010–5090–W, 104.
Moritz, R., Rezeau, H., Ovtcharova, M., Tayan, R., Melkonyan, R., Hovamkimyan, S., Ramazanov, V., Selby, D., Ulianov, A., Chiaradia, M., Putlitz, B., 2016. Long-lived, stationary magmatism and pulsed porphyry systems during Tethyan subduction to postcollision evolution in the southernmost Lesser Caucasus, Armenia and Nakhitchevan. Gondwana Research 37, 465–503.
Mueller, A.G., Muhling, J.R., 2020... Early pyrite and late telluride mineralization in vanadium-rich gold ore from the Oroya Shoot, Paringa South mine, Golden Mile, Kalgoorlie: 3. Ore mineralogy, Pb-Te (Au-Ag) melt inclusions, and stable isotope constraints on fluid sources. Miner. Deposita. https://doi.org/10.1007/s00126-019-00876-6.
Muller D., Groves D.I., 2019. Potassic igneous rocks and associated gold-copper mineralization. Springer International Publishing AG, part of Springer Nature, Berlin-Heidelberg-New York, 5th edition. p. 398.
Mustard, R., Ulrich, T., Kamenetsky, V.S., Mernagh, T., 2006. Gold and metal enrichment in natural granitic melts during fractional crystallization. Geology 34, 85–88.
Newall, P., 2015. NI 43–101 Technical Report on the Initial Mineral Resource Estimate for the Malmyzh Copper-Gold Project. Wardell-Armstrong International Ltd. for Eurasian Minerals Inc. and IG Copper LLC, Khabarovsk Krai, Russian Federation, pp. 160.
Nokleberg, W.J., ed., 2010. Metallogenesis and tectonics of Northeast Asia. U.S. Geological Survey. Prof. Paper 1765. 624 p.
Nokleberg, W.J., Bundtzen, T.K., Dawson, K.M., Eremin, R.A., Goryachev, N.A., Koch, R.D., Ratkin, V.V., Rozenblum, I.S., Shpikerman, V.I., Frolov, Y.F., Gorodinsky, M.E., Melnikov, V.D., Ognyanov, N.V., Petrachenko, E.D., Petrachenko, R.I., Pozdeev, A.I., Ross, K.V., Wood, D.H., Grybeck, D., Khanchuk, A.I., Kovbas, L.I., Nekrasov, I.Y., Sidorov, A.A., 1996. Significant metalliferous and selected non-metalliferous lode deposits and placer districts for the Russian Far East, Alaska, and the Canadian Cordillera. U.S. Geological Survey Open-File Report 96–513-A, 385.
Oakes, C.S., Bodnar, R.J., Simonson, J.M., 1990. The system NaCl-$CaCl_2$-H_2O: 1. The ice liquidus at 1 atm total pressure. Geochim. Cosmochim. Acta 54, 603–610.
Pearce, J., 1996. Sources and settings of granitic rocks. Episodes 19, 120–125.
Pearce, J.A., Harris, N.B.W., Tindle, A.G., 1984. Trace element discrimination diagrams for the tectonic interpretation of granitic rocks. Jour. Petrology 25 (4), 956–983.
Peccerillo, A., Taylor, S.R., 1976. Geochemistry of Eocene calc-alkaline volcanic rocks from the Kastamonu area, Northern Turkey. Contrib. Mineral. Petrol. 58, 63–81.
Petrov, O.V., Kiselev, E.A., Morozov, A.F., Shpikerman, V.I., Zubova, T.N., Shatov, V.V., Zmievsky, Y.P., 2015. State geological mapping, an effective way to the discovery of giant deposits. Regional Geology and Metallogeny 64, 5–10 (in Russian).
Pirajno, F., 2009. Hydrothermal Processes and Mineral Systems. Springer, Berlin, pp. 1250.
Pirajno, F., 2010. Intracontinental strike-slip faults, associated magmatism, mineral systems and mantle dynamics: examples from NW China and Altay-Sayan (Siberia). J. Geodynamics 50, 325–346.
Plotinskaya, O.Y., Grabezhev, A.I., Tessalina, S., Seltmann, R., Groznova, E.O., Abramov,

S.S., 2017. Porphyry deposits of the Urals: Geological framework and metallogeny. Ore Geology Rev. 85, 153–173.
Pollard, P.J., Taylor, R.G., Peters, L., 2005. Ages of intrusion, alteration, and mineralization at the Grasberg Cu-Au deposit, Papua. Indonesia. Econ. Geol. 100, 1005–1020.
Pollard, P.J., Pelenkova, E., Mathur, R., 2017. Paragenesis and Re-Os molybdenite age of the Cambrian Ak-Sug porphyry Cu-Au-Mo deposit, Tyva Republic, Russian Federation. Econ. Geology 112, 1021–1028.
Redmond, P.B., Einaudi, M.T., 2010. The Bingham Canyon porphyry Cu-Mo-Au deposit. I. Sequence of intrusions, vein formation, and sulfide deposition. Econ. Geology 105, 43–65.
Richards, J.P., 2009. Postsubduction porphyry Cu-Au and epithermal Au deposits - products of remelting subduction-modified lithosphere. Geology 37 (3), 247–250.
Richards, J.P., 2011a. Magmatic to hydrothermal metal fluxes in convergent and collided margins. Ore Geology Rev. 40, 1–26.
Richards, J.P., 2011b. High Sr/Y arc magmas and porphyry Cu ± Mo ± Au deposits: Just add water. Econ. Geology 106, 1075–1081.
Roedder, E., 1971. Fluid inclusions studies on the porphyry-type ore deposits at Bingham, Utah, Butte, Montana, and Climax, Colorado. Econ. Geology 66, 98–120.
Roedder, E., 1984. Fluid inclusions in minerals. Rev. Mineral. 12, 644.
Rusk, B.G., Reed, M.H., Dilles, J.H., 2008. Fluid inclusion evidence for magmatic-hydrothermal fluid evolution in the porphyry copper-molybdenum deposit at Butte. Montana. Econ. Geology 103, 307–334.
Sakhno, V.G., Kovalenko, S.V., Alenicheva, A.A., 2011. Monzonitoid magmatism of the Lazurnoe copper-porphyry deposit by the results of U-Pb and K-Ar dating, and peculiarities of the ore-bearing magma genesis by the isotope-geochemical studies. Doklady Earth Sci. 438 (1), 82–90.
Sakhno, V.G., Stepanov, V.A., Gvozdev, V.I., Dobroshevskii, K.N., 2013. The Malinovka gold-bearing ore-magmatic system of central Sikhote Alin (Primor'e Region, Russia): geochronology, petrogeochemistry, and isotopic signatures of igneous complexes. Doklady Earth Sci. 452 (1), 887–894.
Seedorff, E., Dilles, J., Proffett, J.J., Einaudi, M., Zurcher, L., Stavast, W., Johnson, D., Barton, M., 2005. Porphyry deposits: charateristics and origin of hypogene features. Econ. Geology 100, 251–298.
Shashorin, B.N., Makarov, A.I., Rudnev, V.V., Vydrich, D.E., 2018. Geological-geophysical model of the Malmyzh ore-magmatic system and a possibility of its use in the mineral assessment. Subsoil Explor. Protection no.2, 8–16 (in Russian).
Shen, P., Hattori, K., Pan, H., Jackson, S., Seitmuratova, E., 2015. Oxidation condition and metal fertility of granitic magmas: Zircon trace-element data from porphyry Cu deposits in the Central Asian Orogenic Belt. Econ. Geology 110, 1861–1878.
Shinohara, H., Hedenquist, J.W., 1997. Constraints of magma degassing beneath the Far Southeast porphyry Cu-Au deposit, Philippines. Jour. Petrology 38, 1741–1752.
Sillitoe, R.H., 1973. Geology of the Los Pelambres porphyry copper deposit. Chile. Econ. Geology 68, 1–10.
Sillitoe, R.H., 1997. Characteristics and controls of the largest porphyry copper-gold and epithermal gold deposits in the Circum-Pacific region. Austral. Jour. Earth Sci. 44, 373–388.
Sillitoe, R.H., 2000. Gold-rich porphyry deposits: descriptive and genetic models and their role in exploration and discovery. In: Hagemann, S. G., and Brown, P. E. (eds.), Gold in 2000: Reviews in Economic Geology 13, pp. 315–345.
Sillitoe, R.H., 2008. Major gold deposits and belts of the North and South American Cordillera: distribution, tectonomagmatic settings, and metallogenic considerations. Econ. Geology 103, 663–687.
Sillitoe, R.H., 2010. Porphyry copper systems. Econ. Geology 105, 3–41.
Sillitoe R.H., 2010b. Exploration and Discovery of Base- and Precious-metal Deposits in the Circum-Pacific Region – A 2010 Perspective. Resource Geology Special Issue 22. 139 p.
Sillitoe R.H., 2012. Copper provinces. In: Hedenquist J.W., Harris M., Camus F. (eds.), Geology and Genesis of Major Copper Deposits and Districts of the World: A Tribute to Richard H. Sillitoe. SEG Spec. Publ. 16, pp.1-18.
Sillitoe, R.H., Perelló, J., 2005. Andean copper province: Tectonomagmatic settings, deposit types, metallogeny, exploration, and discovery. Econ. Geology 100th Anniv. Vol. 845–890.
Simmons, S.F., White, N.C., John, D.A., 2005. Geological characteristics of epithermal precious and base metal deposits. Econ. Geology 100th Anniv. Vol. 485–522.
Singer, D.A., 1995. World class base and precious metal deposits – a quantitative analysis. Econ. Geology 90, 88–104.
Soloviev, S.G., Krivoschekov, N.N., 2011. The Vostok-2 gold-base metal-tungsten skarn deposit, Central Sikhote-Alin, Russia. Geol. Ore Deposits 6, 543–568.
Soloviev, S.G., Kryazhev, S.G., 2017. Geology, mineralization, and fluid inclusion characteristics of the Skrytoe reduced-type W skarn and stockwork deposit, Sikhote-Alin, Russia. Miner. Deposita 52 (6), 903–928.
Soloviev, S.G., Kryazhev, S.G., Dvurechenskaya, S.S., 2017a. Geology, mineralization, stable isotope, and fluid inclusion characteristics of the Vostok-2 reduced W-Cu skarn and Au-W-Bi-As stockwork deposit, Sikhote-Alin, Russia. Ore Geology Rev. 86, 338–365.
Soloviev, S.G., Kryazhev, S.G., Dvurechenskaya, S.S., 2017b. Geology, mineralization, and fluid inclusion characteristics of the Lermontovskoe reduced-type tungsten (± Cu, Au, Bi) skarn deposit, Sikhote-Alin, Russia. Ore Geology Rev. 89, 15–39.
Soloviev, S.G., Kryazhev, S.G., Avilova, O.V., Andreev, A.V., Girfanov, M.M., Starostin, I.A., 2019. The Lazurnoe deposit in the Central Sikhote-Alin, Eastern Russia: Combined shoshonite-related porphyry Cu-Au-Mo and reduced intrusion-related Au mineralization in a post-subduction setting. Ore Geology Rev. 112 paper 103063.
Sterner, S.M., Hall, D.L., Bodnar, R.J., 1988. Synthetic fluid inclusions - V. Solubility relations in the system NaCl-KCl-H_2O under vapor-saturated conditions. Geochim. Cosmochim. Acta 52, 989–1005.
Sun, W.D., Huang, R.F., Li, H., Hu, Y.B., Zhang, C.C., Sun, S.J., Zhang, L.P., Ding, X., Li, C.Y., Zartman, R.E., Ling, M.X., 2015. Porphyry deposits and oxidized magmas. Ore Geology Rev. 65, 97–131.
Sun, S.-S., McDonough, W.F., 1989. Chemical and isotopic systematics of oceanic basalts: Implications for mantle composition and processes. Geological Society of London, Special Publication 42, 313–345.
Thiéblemont, D., Tegyey, M., 1994. Une discrimination géochimique des roches différenciées témoin de la diversité d'origlisboaine et de situation tectonique des magmas calcoalcalins. Comptes Rendus de l'académie des Sciences Paris 319, 87–94.
Takenouchi, S., Kennedy, G.C., 1965. The solubility of carbon dioxide in NaCl solutions at high temperatures and pressures. Amer. J. Sci. 263, 445–454.
Tsuruoka, S., 2017. The Evolution of Hydrothermal Fluids from the Deep Porphyry Environment to the Shallow Epithermal Environment. Ph. D. Dissertation, Colorado School of Mines 196.
Ulrich, T., Gunther, D., Heinrich, C.A., 1999. Gold concentrations of magmatic brines and the metal budget of porphyry copper deposits. Nature 399, 676–679.
Vanko, D.A., Bodnar, R.J., Sterner, S.M., 1988. Synthetic fluid inclusion: VIII. Vapor-saturated halite solubility in part of the system NaCl-$CaCl_2$-H_2O, with application to fluid inclusions from oceanic hydrothermal systems. Geochim. Cosmochim. Acta 52, 2451–2456.
Vasilenko G.P., 2004. The Dalnegorsk ore district. In: Khanchuk A. I., Gonevchuk G. A., Seltmann R. (Eds.) Metallogeny of the Pacific Northwest (Russian Far East): tectonics, magmatism and metallogeny of active continental margins. Guidebook for the Field Excursions in the Far East of Russia: Sept. 1-20, 2004. Dalnauka, Vladivostok, pp. 98-124.
Vaskin, A.F., Dymovich, V.A., Atrashenko, A.F., Grigoriev, V.B., Zelepugin, V.N., Opalikhina, E.S., Sharov, L.A., Leontieva, L.Y., 2009. Explanatory notes to the geological map of Russia, M-53 map sheet, 1: 1,000,000 scale, 3rd generation. VSEGEI, St-Petersburg. 376 (in Russian).
White, N.C., Hedenquist, J.W., 1995. Epithermal gold deposits: styles, characteristics and exploration. SEG Newsletter 23, 1–9.
Wilkinson, J., Chang, Z., Cooke, D., Baker, M., Wilkinson, C., Inglis, S., Chen, H., Gemmell Jr., B., 2015. The chlorite proximator: a new tool for detecting porphyry ore deposits. J. Geochem. Explor. 152, 10–26.
Williams-Jones, A.E., Heinrich, C.A., 2008. Vapor transport of metals and the formation of magmatic-hydrothermal ore deposits. Econ. Geology 100, 1287–1312.
Wilson, A.J., Cooke, D.R., Harper, B.L., 2003. The Ridgeway gold-copper deposit; a high-grade alkalic porphyry deposit in the Lachlan fold belt, New South Wales, Australia. Econ. Geology 98, 1637–1666.
Yang, F., Mao, J., Pirajno, F., Yan, S., Liu, G., Zhou, G., Zhang, Z., Liu, F., Geng, X., Guo, C., 2012. A review of the geological characteristics and geodynamic setting of Late Paleozoic porphyry copper deposits in the Junggar region, Xinjiang Uygur Autonomous Region, Northwest China. J. Asian Earth Sci. 49, 80–98.
Yang, X.-M., 2012. Sulfur solubility in felsic magmas: implications for genesis of intrusion-related gold mineralization. Geosci. Canada 39, 17–32.
Zhang, X., Spry, P.G., 1994. Calculated stability of aqueous tellurium species, calaverite and hessite at elevated temperatures. Econ. Geology 89, 1152–1166.